Renormalization group improved m_s and $|V_{us}|$ determination from hadronic τ decays

B. Ananthanarayan,[1,*] Diganta Das,[2,†] and M. S. A. Alam Khan[1,‡]

[1]*Centre for High Energy Physics, Indian Institute of Science, Bangalore 560 012, India*
[2]*Center for Computational Natural Sciences and Bioinformatics, International Institute of Information Technology, Hyderabad 500 032, India*

(Received 7 July 2022; accepted 9 December 2022; published 30 December 2022)

We determine the strange quark mass (m_s) and quark mixing element $|V_{us}|$, and their joint determination from the Cabibbo suppressed hadronic τ decays in various perturbative schemes. We improve this analysis compared to the previous analysis based on the optimal renormalization or the renormalization group summed perturbation theory (RGSPT) scheme by replacing the theoretical longitudinal contributions with phenomenological parametrization; the RGSPT coefficients are used for the dimension-4 Adler functions. The improved analysis results in the extraction of $m_s(2\ \mathrm{GeV}) = 98 \pm 19\ \mathrm{MeV}$ and $|V_{us}| = 0.2191 \pm 0.0043$ from the RGSPT scheme.

DOI: 10.1103/PhysRevD.106.114036

I. INTRODUCTION

The hadronic decays of the τ leptons have been of constant interest for determining various parameters of the Standard Model (SM) of particle physics. The availability of experimental data on the strange and nonstrange decay modes for the hadronic τ decays has opened the window for the determination of various parameters relevant for quantum chromodynamics (QCD), namely, the strong coupling constant α_s, the strange quark mass m_s, the vacuum condensates, the low-energy chiral couplings, and the quark mixing element $|V_{us}|$ of the Cabibbo-Kobayashi-Maskawa (CKM) matrix (see Refs. [1,2] for details).

On the theoretical side, the QCD contributions to the hadronic τ decays are studied by evaluating the current correlator using operator product expansion (OPE) [3]. The OPE factorizes the long- and short-distance contributions. The long-distance information is encoded into the vacuum condensates. The short-distance part is written as the perturbative series in the strong coupling constant and quark masses. The vacuum condensates can also be evaluated using chiral perturbation theory (ChPT) [4], lattice QCD [5], and renormalization group (RG) optimized perturbation theory [6,7]. The short-distance contributions require evaluation of the Feynman diagrams. It is also known that some of the contributions to the hadronic vacuum polarization function are not captured by the OPE, which is a quark-hadron duality violation. These duality violating terms are parametrized in a model-dependent way and fitted to experimental data and should also be added to the OPE contributions [8].

The longitudinal component of the QCD Adler function, corresponding to the zero angular momentum state, has been calculated to $\mathcal{O}(\alpha_s^4)$ [9–14]. It has poor convergence behavior and raises the question of the method's applicability in the extraction of strange quark mass. This problem can be solved by replacing these contributions with their phenomenological input, and it has been used in Refs. [15–19] for m_s and $|V_{us}|$ extractions from the experimental moment data. These improvements have resulted in much better control over the theoretical uncertainties in the m_s and $|V_{us}|$ determinations.

The hadronic τ decays have been extensively studied using various perturbative schemes. These schemes differ in how the strong coupling constant and quark masses are evaluated along the contour in the complex plane using their RG properties. The most commonly used schemes in the extraction of the strange quark mass and CKM matrix element from the Cabibbo suppressed hadronic τ decay are fixed-order perturbation theory (FOPT) and contour improved perturbation theory (CIPT). For the hadronic τ decays, the FOPT suffers from the problem of large logarithms along the contour in the complex energy plane, and the higher-order spectral moments are very sensitive to scale variations. In the CIPT scheme, direct numerical

*anant@iisc.ac.in
†diganta.das@iiit.ac.in
‡alam.khan1909@gmail.com

evaluation of coupling constants and masses along the complex contour using their RGE does not suffer from the problem of large logarithms. However, scale dependence is still the major source of theoretical uncertainties for higher moments.

Recently, the optimal renormalization or RG summed perturbation theory (RGSPT) has been used by two of us in Ref. [20] in the strange quark mass determination. The behavior of polarization and Alder functions in the complex contour was also studied for RGSPT, CIPT, FOPT, and the method of effective charges (MEC) in great detail. However, the numerical impact of theoretical uncertainties from perturbation series truncation and scale dependence was excluded. We improve the previous analysis in the following ways:

(i) We include the RGSPT coefficients for dimension-4 Adler functions.
(ii) We replace the divergent longitudinal perturbative QCD expressions for the Adler function with the phenomenological parametrization used in Refs. [15,17]. This replacement significantly reduces the theoretical uncertainties.
(iii) We perform $|V_{us}|$ as well as the joint m_s and $|V_{us}|$ determinations for the first time using RGSPT.
(iv) The effects of the variation of m_s and $|V_{us}|$ with the variation of the moments calculated at different energies ($s_0 < M_\tau^2$) are also included and found to constitute an important source of uncertainty.
(v) We use the five-loop QCD β function and anomalous dimensions for the running of the strong coupling constant and quark masses.

The article is organized as follows: Sec. II provides a brief overview of the various quantities that are needed for the extraction of m_s and $|V_{us}|$. A short introduction to RGSPT is given in Sec. III. Section IV explains the OPE contributions to the Adler function. The behavior of leading-order mass corrections to the Adler functions in different schemes used in this article is studied in Sec. V. The higher-order term of the perturbation series becomes very important for the higher moments, and two prescriptions for the truncation of the perturbation series are also defined in this section. In Sec. VI, the phenomenological parametrization of longitudinal contributions is briefly discussed. Then, we move to Sec. VII, where strange quark mass is extracted using only the perturbative QCD (pQCD) contributions calculated from OPE. The weighted average results for the $m_s(M_\tau^2)$ extraction using this method in the CIPT, FOPT, and RGSPT schemes are presented in Table IV. The details of uncertainties can be found in Appendix E 1. In Sec. VIII, the $m_s(M_\tau^2)$ determination using the phenomenological parametrization for the longitudinal component is performed, and results are presented in Table V. Details of the strange quark mass determinations from the moments are presented in Appendix E 2. The determination of $|V_{us}|$ using external input for m_s is performed in Sec. IX. The weighted average results using the OPAL and ALEPH data are presented in Tables VIII and VI, respectively. The details of determinations from the moments, as well as the uncertainties coming from various sources, are presented in Appendix E 3. In Sec. X, the joint extraction of m_s and $|V_{us}|$ is performed. We provide a summary and conclusion in Sec. XI. We also provide supplementary input needed for this article in Appendixes A–D. The details of the m_s and $|V_{us}|$ determinations from the moments can be found in Appendix E.

II. FORMALISM

An important quantity for the study of hadronic τ decay widths [21–23] is the two-point current correlator:

$$\Pi^{V/A}_{\mu\nu,ij}(p^2) \equiv i \int dy e^{ipy} \langle \Omega | T\{J^{V/A}_{\mu,ij}(y) J^{V/A}_{\nu,ij}(0)^\dagger\} | \Omega \rangle \qquad (1)$$

where $|\Omega\rangle$ denotes the physical vacuum, $J^{V/A}_{\mu,ij}(y) = (\bar{q}_j \gamma_\mu / (\gamma_\mu \gamma_5) q_i)(x)$ is the hadronic vector/axial current, and the indices i and j denote the flavors of light quarks. The current correlator can be calculated perturbatively using OPE [3] as a power expansion in $1/p$, and the corresponding coefficients are the operators of that dimension. Purely perturbative corrections appear up to dimension 2 in the OPE expansion, and the long-distance corrections corresponding to the vacuum condensates start from dimension 4.

Using Lorentz decomposition, the current correlator in Eq. (1) can be decomposed into the longitudinal and transverse components with angular momentum $J = 0$ and $J = 1$ as

$$\Pi^{V/A}_{\mu\nu,ij}(p^2) = (p_\mu p_\nu - g_{\mu,\nu}) \Pi^{V/A,T}_{ij}(p^2) + p_\mu p_\nu \Pi^{V/A,L}_{ij}(p^2). \qquad (2)$$

The L/T correlators are related to the experimentally measurable semihadronic τ decay rate (R_τ), defined by

$$R_\tau \equiv \frac{\Gamma(\tau^- \to \text{hadrons}\, \nu_\tau(\gamma))}{\Gamma(\tau^- \to e^- \nu_\tau(\gamma))} = R_{\tau,V} + R_{\tau,A} + R_{\tau,S}, \qquad (3)$$

and they are related to the imaginary part of the current correlators in Eq. (2) by

$$R_\tau(s_0) = 12\pi \int_0^{s_0} \frac{ds}{s_0} \left(1 - \frac{s}{s_0}\right)^2 \times \left[\left(1 + \frac{2s}{s_0}\right) \mathrm{Im}(\Pi^T)(s) + \mathrm{Im}(\Pi^L)(s)\right]. \qquad (4)$$

It should be noted that these current correlators also carry information about mixing among the quark flavors and can be written as

$$\Pi^J \equiv \sum_{i=d,s} |V_{ui}|^2 [\Pi^{V,J}_{ui}(s) + \Pi^{A,J}_{ui}(s)], \tag{5}$$

and $|V_{ij}|$ are the elements of the CKM matrix.

To study the invariant mass distribution of final-state hadrons, we need moments from the hadronic τ decay rate, defined by [24]

$$R^{kl}_\tau(s_0) \equiv \int_0^{s_0} ds \left(1 - \frac{s}{s_0}\right)^k \left(\frac{s}{s_0}\right)^l \frac{dR_\tau}{ds}. \tag{6}$$

Using integration by parts, we can convert Eq. (6) into the following form:

$$R^{kl}_\tau(s_0) = -i\pi \oint_{|x_c|=1} \frac{dx_c}{x_c} \times \{3\mathcal{F}^{L+T}_{kl}(x_c)\mathcal{D}^{L+T}(s_0 x_c) + 4\mathcal{F}^{L}_{kl}(x_c)\mathcal{D}^{L}(s_0 x_c)\}, \tag{7}$$

where $x_c = s/s_0$ and $\mathcal{D}^{L+T}(s)$ are the Adler functions.

In the literature, the experimental values of the moments defined above are usually provided for $s_0 = M_\tau^2$. However, their values at different energies can be calculated using the experimental data on the spectral functions provided in Refs. [25–28].

The Adler function satisfies the homogeneous renormalization group equation (RGE) and is related to the current correlators by the relation

$$\mathcal{D}^{L+T}(s) \equiv -s\frac{d}{ds}(\Pi^{L+T}(s)), \tag{8}$$

$$\mathcal{D}^{L}(s) \equiv \frac{s}{M_\tau^2}\frac{d}{ds}(s\Pi^{L}(s)). \tag{9}$$

The resulting quantity in Eq. (7) is an expansion in the strong coupling constant, quark masses, and condensates of higher dimension operators. It explicitly depends on the CKM matrix element and the electroweak corrections. These terms are not shown in Eq. (7) but are factored out in Eqs. (12) and (13). The kinematic kernels $\mathcal{F}^{kl}_{L+T}(x_c)$ and $\mathcal{F}^{kl}_{L}(x_c)$ appearing in the Eq. (7) are given by

$$\mathcal{F}^{kl}_{L+T}(x_c) \equiv 2(1-x_c)^{3+k} \sum_{n=0}^{l} \frac{l!}{(l-n)!n!}(x_c-1)^n \times \frac{(6+k+n)+2(3+k+n)x_c}{(3+k+n)(4+k+n)}, \tag{10}$$

$$\mathcal{F}^{kl}_{L}(x_c) \equiv 3(1-x_c)^{3+k} \sum_{n=0}^{l} \frac{l!}{(l-n)!n!}\frac{(x_c-1)^n}{(3+k+n)}, \tag{11}$$

and their explicit form used in this article is presented in Table I.

TABLE I. Kinematic kernels used in this article.

(k,l)	$\mathcal{F}^{kl}_{L+T}(x)$	$\mathcal{F}^{kl}_{L}(x)$
(0, 0)	$(1-x)^3(1+x)$	$(1-x)^3$
(1, 0)	$\frac{1}{10}(1-x)^4(7+8x)$	$\frac{3}{4}(1-x)^4$
(2, 0)	$\frac{2}{15}(1-x)^5(4+5x)$	$\frac{3}{5}(1-x)^5$
(3, 0)	$\frac{1}{7}(1-x)^6(3+4x)$	$\frac{1}{2}(1-x)^6$
(4, 0)	$\frac{1}{14}(1-x)^7(5+7x)$	$\frac{3}{7}(1-x)^7$

Performing the contour integral defined in Eq. (7), we can write R^{kl}_τ [21] as

$$R^{kl}_\tau(s_0) = 3(|V_{ud}|^2 + |V_{us}|^2)S_{\rm EW}\{1 + \delta'_{\rm EW} + \delta^{(0),kl} + \sum_{n=2,4\ldots} (\cos^2(\theta_C)\delta^{(n),kl}_{ud} + \sin^2(\theta_C)\delta^{(n),kl}_{us})\}, \tag{12}$$

where $\theta_C = \sin^{-1}(|V_{us}|/\sqrt{(|V_{us}|^2+|V_{ud}|^2)})$ is the Cabibbo angle, $\delta^{(n)}_{ud,us}$ [21] carry information about the contour integrals evaluated in Eq. (7), and $\delta'_{\rm EW} = 0.0010$ and $S_{\rm EW} = 1.0201 \pm 0.0003$ are one-loop RG improved electroweak corrections [29,30].

The most important quantity of interest in the determination of the strange quark mass is the $SU(3)$ breaking term $\delta R^{kl}_\tau(s_0)$ [31] defined as

$$\delta R^{kl}_\tau(s_0) \equiv \frac{R^{kl}_{\tau,V+A}(s_0)}{|V_{ud}|^2} - \frac{R^{kl}_{\tau,S}(s_0)}{|V_{us}|^2} \tag{13}$$

$$= 3S_{\rm EW}\sum_{n\geq 2}(\delta^{(n),kl}_{ud} - \delta^{(n),kl}_{us}), \tag{14}$$

which is free from instanton and renormalon contributions and vanishes in the chiral limit. It is an experimentally measurable quantity with input taken from Table II along with the theoretical quantities appearing in Eq. (13) in the strange quark mass determination.

The value of the strong coupling constant $\alpha_s(M_Z^2) = 0.1179 \pm 0.0010$ has been taken from Ref. [33] and evolved to the τ lepton mass scale using a five-loop β function from the package REvolver [34]. Its value at the τ

TABLE II. Spectral moments from ALEPH [31,32] and OPAL [27]. OPAL moments are calculated using the current value of $|V_{us}| = 0.2243 \pm 0.0008$ quoted in the PDG [33].

	δR^{kl}_τ	
Moments (k,l)	ALEPH	OPAL
(0, 0)	0.374 ± 0.133	0.332 ± 0.10
(1, 0)	0.398 ± 0.077	0.326 ± 0.078
(2, 0)	0.399 ± 0.053	0.340 ± 0.058
(3, 0)	0.396 ± 0.042	0.353 ± 0.046
(4, 0)	0.395 ± 0.034	0.367 ± 0.037

lepton mass is $\alpha_s(M_\tau^2) = 0.3187 \pm 0.0083$, which has been used in this article.

III. REVIEW OF OPTIMAL RENORMALIZATION

The optimal renormalization technique is used to resum the running logarithms present in the perturbation series using RGE [35–37]. The resulting summed series shows reduced scale dependence and hence a reduction in the theoretical uncertainty in the extraction of a quantity of interest. In the case of hadronic τ decays, where weighted integrals along the complex contour are involved, these running logarithms become very important. Their summation is necessary to perform the perturbative analysis properly. RGSPT resums these logarithms, and the resulting fixed-order truncated series has less sensitivity to scale variations even for higher moments than FOPT and CIPT.

The perturbative series describing a QCD process is given by

$$W(x,m) = x^{n_1} m^{n_2} \sum_{i=0} x^i L^j T_{i,j}, \tag{15}$$

where $x \equiv x(\mu^2)$, $L \equiv \log(\mu^2/q^2)$ and $m = m(\mu^2)$. We can rewrite the series as follows:

$$W^{RG\Sigma} = x^{n_1} m^{n_2} \sum_{i=0} x^i S_i[xL], \tag{16}$$

where the $S_i[xL]$ coefficients are given by

$$S_i[xL] = \sum_{n=i}^{\infty} T_{n,n-i} (xL)^{n-i}. \tag{17}$$

The RGE for Eq. (15) is given by

$$\mu^2 \frac{d}{d\mu^2} W(x,m) - \gamma_a(x) W(x,m) = 0, \tag{18}$$

$$(\beta(x)\partial_x + \gamma_m(x)\partial_m + \partial_L - \gamma_a(x)) W(x,m) = 0, \tag{19}$$

where $\gamma_a(x) = \sum_{i=0} x^{i+1} \gamma_a^{(i)}$ is the anomalous dimension associated with $W(x,m)$. The RGSPT version of the coefficients ($\tilde{q}_i, \tilde{h}_i, \tilde{g}_n, \tilde{j}_n$ and $\tilde{k}_n$) relevant for Eqs. (33) and (34) are presented in Appendix C. Using the numerical values from Refs. [59,33,60]. We can collect the terms corresponding to summed coefficients defined in Eq. (17). This process results in a set of coupled differential equations for $S_i[w]$, which can be summarized as

$$\sum_{i=0}^{n} [\beta_i(\delta_{i,0} + w - 1) S'_{n-i}(w) + S_{n-i}(w)(n_2\gamma_i + \beta_i(n_1 - i + n) + \gamma_a^{(i)})] = 0. \tag{20}$$

Here we have substituted $w = 1 - \beta_0 xL$, which simplifies the solutions of differential equations. For further details on RG summation, we refer to Refs. [20,35–40].

The solution to the first three summed coefficients—relevant for dimension-0 and dimension-2 Adler functions—appearing in Eq. (20) can be found in Appendix B. It should be noted that the RGEs for dimension-4 operators mix perturbative coefficients with condensates; hence, they do not obey Eq. (16).

IV. OPE CONTRIBUTIONS TO THE QCD ADLER FUNCTION

A. Leading-order contribution

Dimension zero is the leading perturbative contribution to the current correlator in the massless limit, and it has been calculated to $\mathcal{O}(\alpha_s^4)$ [41–50]. It receives a contribution only from the transverse piece of the current correlator, which is identical for both vector and axial-vector channels and thus cancels in Eq. (13). The Adler functions obtained using the OPE can be organized as follows:

$$\mathcal{D}^{L+T}(s) = \sum_{n=0,2,4,\cdots} \frac{1}{s^{\frac{n}{2}}} \mathcal{D}_n^{L+T}(s), \tag{21}$$

$$\mathcal{D}^{L}(s) = \frac{1}{M_\tau^2} \sum_{n=2,4,\cdots} \frac{1}{s^{\frac{n}{2}-1}} \mathcal{D}_n^{L}(s), \tag{22}$$

where ij are the flavor indices and the Adler functions in the rhs of the above equations are expansions in α_s, m_q, and the quark and gluon condensate terms. Their definition gets clearer if we take a contour integration along $s = M_\tau^2 e^{i\phi}$, and the coefficients of $(M_\tau^2)^{-n}$ are called operators of dimension $2n$. The massless Adler functions are given by

$$\mathcal{D}_0^{L+T,V/A}(s) = \frac{1}{4\pi} \sum_i x(-s)^i \tilde{K}_i^{L+T}, \tag{23}$$

$$\mathcal{D}_0^{L,V/A}(s) = 0, \tag{24}$$

where $x(-s) = x(q^2) = \alpha_s(q^2)/\pi$ and $\tilde{K}_i^{L+T}$ are the coefficients of the Adler function at the ith loop, which can be found in Appendix D. The RG running of the dimension-zero "$L+T$" component of the Adler function is given by

$$\mu^2 \frac{d}{d\mu^2} \mathcal{D}_0^{L+T,V/A}(s) = \left(\beta(x)\frac{\partial}{\partial x} + \frac{\partial}{\partial L}\right) \mathcal{D}_0^{L+T,V/A}(s) = 0, \tag{25}$$

where $L = \log(\frac{\mu^2}{-s})$, and the QCD beta function $[\beta(x)]$ is defined as

$$\mu^2 \frac{d}{d\mu^2} x(\mu^2) = \beta(x(\mu^2)) = -\sum_i \beta_i x(\mu^2)^{i+2}. \tag{26}$$

The coefficients of the beta function β_i's are known up to five loops and are presented in Appendix A.

B. Dimension-2 contributions to the Adler function

The leading-order mass corrections to the hadronic τ decay rate come from the dimension-2 Adler function. The $\mathcal{D}^{L+T}(s)$ Adler function is known to $\mathcal{O}(\alpha_s^3)$ [51–56] while $\mathcal{D}^{L}$ is known to $\mathcal{O}(\alpha_s^4)$ [9–14], and their analytic expression can be found in Appendix D 2. The RG running of dimension-2 operators is given by

$$\mu^2\frac{d}{d\mu^2}\mathcal{D}_2^J(s)=\left\{\frac{\partial}{\partial L}+\beta(x(\mu^2))\frac{\partial}{\partial x(\mu^2)}+2\gamma_m(x(\mu^2))\frac{\partial}{\partial m_i(\mu^2)}\right\}\mathcal{D}_2^J(s)=0, \quad (27)$$

where the QCD beta function and the quark mass anomalous dimension (γ_m) are known to five loops and can be found in Appendix A.

The $SU(3)$ breaking contributions from the Adler function in the determination of quark masses is the difference

$$\delta\mathcal{D}_2^{J,V+A}(s)\equiv\mathcal{D}_{2,ud}^{J,V+A}(s)-\mathcal{D}_{2,us}^{J,V+A}(s), \quad (28)$$

where $J=(L+T)/L$ and the analytic expressions can be found in Appendix D 2. These contributions are used in Eq. (13) to evaluate the leading-order mass correction term $\delta_{ud}^{(2),kl}-\delta_{us}^{(2),kl}$.

The absence of a coefficient $\mathcal{O}(\alpha_s^4)$ for the "$L+T$" Adler function induces an additional theoretical uncertainty in the predictions from perturbation theory. This missing piece can be estimated by $\tilde{d}_4^{L+T}\sim(\tilde{d}_3^{L+T})^2/\tilde{d}_2^{L+T}\approx 4067$, which is used in the strange quark mass determinations in this article.

The renormalization group running of different coefficients for CIPT and FOPT coefficients can be found in Refs. [22,57]. The RG summed coefficients can be obtained from Appendix B by setting $\{n_1,n_2\}=\{0,2\}$.

C. Dimension-4 contributions to the Adler function

The OPE expansion at dimension 4 involves contributions from perturbative, quark, and gluon condensates [22,58]. However, these contributions are suppressed by a factor of $(\frac{1}{M_\tau^2})^2$, and they have the following form:

$$\mathcal{D}_{4,ij}^{L+T,V/A}(s)=\frac{1}{s^2}\sum_{n=0}\tilde{\Omega}_n^{L+T}(s)x(-s)^n, \quad (29)$$

$$\mathcal{D}_{4,ij}^{L,V/A}(s)=\frac{1}{M_\tau^2 s}\left\{\frac{3}{2\pi^2}\sum_{n=0}\tilde{\Omega}_n^{L}(s)x(-s)^n-\langle(m_i\mp m_j)(\bar{q}_iq_i\mp\bar{q}_jq_j)\rangle\right\}, \quad (30)$$

where the upper/lower sign corresponds to the V/A component. The $\tilde{\Omega}^{L+T/L}$ coefficients are given by

$$\begin{aligned}\tilde{\Omega}^{L+T}(s)=&\frac{1}{6}\langle G^2\rangle+2\langle m_i\bar{q}_iq_i+m_j\bar{q}_jq_j\rangle\tilde{q}_n^{L+T}\\&\pm\frac{8}{3}\langle m_j\bar{q}_iq_i+m_i\bar{q}_jq_j\rangle\tilde{t}_n^{L+T}+\sum_k\langle m_k\bar{q}_kq_k\rangle\\&-\frac{3}{\pi^2}\Big\{(m_i^4+m_j^4)\tilde{h}_n^{L+T}-m_i^2m_j^2\tilde{g}_n^{L+T}\\&\pm\frac{5}{3}m_im_j(m_i^2+m_j^2)\tilde{k}_n^{L+T}+\sum_k m_k^4\tilde{j}_n^{L+T}\\&+2\sum_{k\neq l}m_k^2m_l^2\tilde{u}_n^{L+T}\Big\},\end{aligned} \quad (31)$$

$$\tilde{\Omega}^{L}(s)=(m_i^2+m_j^2)\tilde{h}_n^{L}\pm\frac{3}{2}m_im_j\tilde{k}^{L}+\sum_k m_k^2\tilde{j}_n^{L}, \quad (32)$$

where $\langle m_i\bar{q}_jq_j\rangle\equiv\langle 0|m_i\bar{q}_jq_j|0\rangle(-\xi^2 s)$, $m_i=m_j(-\xi^2 s)$, $\langle G^2\rangle\equiv\langle 0|G^2|0\rangle(-\xi^2 s)$, and ξ is the scale parameter used to keep track of the dependence of the renormalization scale. The RG evolution of the perturbative coefficients and the condensates can be found in Ref. [22].

The relevant OPE corrections to the strange quark mass determination are as follows:

$$\begin{aligned}\delta\mathcal{D}_4^{L+T}(s)\equiv&\mathcal{D}_{4,ud}^{L+T,V+A}(s)-\mathcal{D}_{4,us}^{L+T,V+A}(s)\\=&\frac{-4\delta O_4}{s^2}\sum_{n=0}\tilde{q}_n^{L+T}x(-s)^n+\frac{6}{\pi^2s^2}m_s(-s)^4(1-\epsilon_d^2)\\&\times\sum_{n=0}\{(1+\epsilon_d^2)\tilde{h}_n^{L+T}-\epsilon_u^2\tilde{g}_n^{L+T}\}x(-s)^n,\end{aligned} \quad (33)$$

$$\begin{aligned}\delta\mathcal{D}_4^{L}(s)\equiv&\mathcal{D}_{4,ud}^{L,V+A}(s)-\mathcal{D}_{4,us}^{L,V+A}(s)\\=&\frac{2\delta O_4}{sM_\tau^2}-\frac{3}{\pi^2sM_\tau^2}m_s^4(1-\epsilon_d^2)\\&\times\sum_{n=0}\{(1+\epsilon_d^2)(\tilde{h}_n^{L}+\tilde{j}_n^{L})+\epsilon_u^2(2\tilde{h}_n^{L}-3\tilde{k}_n^{L}+\tilde{j}_n)\}\\&\times x(-s)^n,\end{aligned} \quad (34)$$

where $\delta O_4=\langle 0|m_s\bar{s}s-m_d\bar{d}d|\rangle(-\xi^2 s)$ with $\epsilon_u=m_u/m_s$ and $\epsilon_u=m_u/m_s$. Using the numerical values

$$\begin{aligned}&v_s=0.738\pm0.029\quad[59],\\&f_\pi=92.1\pm0.8\ \text{MeV},\qquad m_\pi=139.6\ \text{MeV}\quad[33]\\&\epsilon_d=0.053\pm0.002,\qquad \epsilon_u=0.029\pm0.003\quad[60],\end{aligned} \quad (35)$$

δO_4 can be estimated similarly to Ref. [22] as

$$\begin{aligned}\delta O_4 &= (v_s m_s - m_d)\langle 0|\bar{d}d|0\rangle \\ &\simeq -\frac{m_s}{2\hat{m}}(v_s - \epsilon_d) f_\pi^2 m_\pi^2 \\ &= -(1.54 \pm .08) \times 10^3 \text{ GeV}^{-4}. \end{aligned} \tag{36}$$

V. BEHAVIOR OF LEADING-ORDER PERTURBATIVE MASS CORRECTIONS IN DIFFERENT RENORMALIZATION SCHEMES

FOPT and CIPT are the versions of perturbative theory for the QCD analysis of the τ decay frequently used in the literature, and they have been further extended by including a RGSPT version of perturbation theory [20,38]. It has been shown in Ref. [38] that the $\delta^{(0)}$ contributions from the RGSPT scheme approach CIPT at higher orders of perturbation theory, and the corresponding numerical value of the strong coupling constant lies closer to the CIPT value. Similar behavior is also observed in this article for the higher dimensional operators, but with the advantage that the scale dependence for higher moments is under control in the case of RGSPT compared to FOPT and CIPT. Before moving on to the strange quark mass determination, the convergence behavior of the leading-order mass corrections must be analyzed carefully for different schemes. This exercise is performed in the rest of the section.

The leading-order mass corrections to moment $\delta R_\tau^{kl,2}$ in Eq. (13) are given by

$$\delta R^{kl,D=2} = 24 \frac{m_s(\xi^2 M_\tau^2)^2}{M_\tau^2} S_{\rm EW}(1 - \epsilon_d^2)\Delta_{kl}(x,\xi), \tag{37}$$

where

$$\Delta_{kl}(x,\xi) \equiv \left(\frac{3}{4}\Delta_{kl}^{L+T}(x,\xi) + \frac{1}{4}\Delta_{kl}^{L}(x,\xi)\right), \tag{38}$$

and $\Delta_{kl}^{J}(x,\xi)$ are the contributions from the Adler functions $\delta\mathcal{D}^J$ involving Eqs. (D5), (D8), and (D11) evaluated along a contour in the complex plane with the kernels presented in Table I. These functions are calculated differently in various schemes as explained in the later subsections.

It should be noted that the leading-order mass corrections are presented to remember where the perturbative series is truncated in prescription I.

A. CIPT scheme

In CIPT, the masses and the strong coupling evolve along the contour in the complex plane by solving the RGE numerically. By construction, it does not suffer from the problem of a large logarithm along the contour. Following Refs. [22,57,61], the dimension-2 contribution to the $L+T$-component moments can be organized in terms of contour integrals:

$$\begin{aligned}\Delta_{kl}^{L+T}(x,\xi) = -\frac{1}{4\pi i}\sum_{n=0}\tilde{d}_n^{L+T}(\xi)\oint_{|x_c|=1}\frac{dx_c}{x_c^2}\mathcal{F}_{kl}^{L+T}(x_c) \\ \times \frac{m_s^2(-\xi^2 M_\tau^2 x_c)}{m_s^2(M_\tau^2)} x^n(-\xi^2 M_\tau^2 x_c), \end{aligned} \tag{39}$$

and for the longitudinal component,

$$\begin{aligned}\Delta_{kl}^{L}(x,\xi) = \frac{1}{2\pi i}\sum_{n=0}\tilde{d}_n^{L}(\xi)\oint_{|x_c|=1}\frac{dx}{x_c}\mathcal{F}_{kl}^{L}(x_c) \\ \times \frac{m_s^2(-\xi^2 M_\tau^2 x)}{m_s^2(M_\tau^2)} x^n(-\xi^2 M_\tau^2 x_c). \end{aligned} \tag{40}$$

The dimension-2 contributions to Δ_{kl}^{L+T} for $x(M_\tau^2) = 0.3187/\pi$ contributions of different orders are given by

$$\begin{aligned}\Delta_{0,0}^{L+T} &= \{0.7717, 0.2198, 0.0777, -0.0326, -0.135\}, \\ \Delta_{1,0}^{L+T} &= \{0.9247, 0.3324, 0.1951, 0.0866, -0.0375\}, \\ \Delta_{2,0}^{L+T} &= \{1.0605, 0.4410, 0.3202, 0.2302, 0.1019\}, \\ \Delta_{3,0}^{L+T} &= \{1.1883, 0.5504, 0.4567, 0.4021, 0.2897\}, \\ \Delta_{4,0}^{L+T} &= \{1.3130, 0.6634, 0.6073, 0.6065, 0.5337\}, \end{aligned} \tag{41}$$

which shows good convergence up to the (2, 0) moment. The longitudinal contributions are

$$\begin{aligned}\Delta_{0,0}^{L} &= \{1.6031, 1.1990, 1.1583, 1.3023, 1.6245\}, \\ \Delta_{1,0}^{L} &= \{1.3832, 1.1358, 1.1970, 1.4642, 1.9856\}, \\ \Delta_{2,0}^{L} &= \{1.2563, 1.1158, 1.2635, 1.6553, 2.4004\}, \\ \Delta_{3,0}^{L} &= \{1.1783, 1.1204, 1.3494, 1.8740, 2.8757\}, \\ \Delta_{4,0}^{L} &= \{1.1301, 1.1418, 1.4517, 2.1216, 3.4196\}, \end{aligned} \tag{42}$$

and we can see that longitudinal contributions show divergent behavior. The total perturbative contributions of dimension 2 obtained using Eq. (38) are

$$\begin{aligned}\Delta_{0,0} &= \{0.9795, 0.4646, 0.3478, 0.3011, 0.3050\}, \\ \Delta_{1,0} &= \{1.0393, 0.5333, 0.4456, 0.4310, 0.4682\}, \\ \Delta_{2,0} &= \{1.1094, 0.6097, 0.5560, 0.5865, 0.6765\}, \\ \Delta_{3,0} &= \{1.1858, 0.6929, 0.6799, 0.7701, 0.9362\}, \\ \Delta_{4,0} &= \{1.2673, 0.7830, 0.8184, 0.9853, 1.2552\}. \end{aligned} \tag{43}$$

It is clear from Eq. (43) that the pathological longitudinal contributions are a restricting factor in getting any reliable determination from CIPT unless we truncate the perturbative series to the minimum term.

B. FOPT scheme

In FOPT, the perturbative series for the Adler function is truncated to a given order in $\alpha_s(\mu)$, and running logarithms are integrated analytically along the contour in the complex energy plane [57,62]. The Δ^J_{kl} for FOPT is evaluated by inserting Eqs. (D6) and (D9) into Eq. (37) and can be written as

$$\Delta^J_{kl}(x,\xi) = \sum_{i=0}^{4}\sum_{j=0}^{i} x^i(\xi^2 M_\tau^2)\tilde{d}^J_{i,j} H^{kl,J}_j(x,\xi), \quad (44)$$

where $H^{kl,J}_i(\xi)$ are evaluated analytically:

$$H^{kl,L+T}_n(x,\xi) \equiv \frac{-1}{4\pi i}\oint_{|x_c|=1}\frac{dx_c}{x_c^2}\mathcal{F}^{L+T}_{kl}(x_c)\log^n\left(\frac{-\xi^2}{x_c}\right), \quad (45)$$

$$H^{kl,L}_n(x,\xi) \equiv \frac{1}{2\pi i}\oint_{|x_c|=1}\frac{dx_c}{x_c}\mathcal{F}^{L}_{kl}(x_c)\log^n\left(\frac{-\xi^2}{x_c}\right). \quad (46)$$

Evaluating the above integrals, the Δ^{L+T}_{kl} contribution, using FOPT, at different orders of perturbative series is given by

$$\begin{aligned}
\Delta^{L+T}_{0,0} &= \{1.0000, 0.4058, 0.2575, 0.1544, 0.0163\},\\
\Delta^{L+T}_{1,0} &= \{1.0000, 0.5072, 0.4168, 0.3679, 0.2971\},\\
\Delta^{L+T}_{2,0} &= \{1.0000, 0.5782, 0.5366, 0.5414, 0.5429\},\\
\Delta^{L+T}_{3,0} &= \{1.0000, 0.6323, 0.6330, 0.6892, 0.7636\},\\
\Delta^{L+T}_{4,0} &= \{1.0000, 0.6758, 0.7140, 0.8189, 0.9654\}. \quad (47)
\end{aligned}$$

The Δ^L_{kl} are given by

$$\begin{aligned}
\Delta^{L}_{0,0} &= \{1.0000, 0.9468, 1.1319, 1.3807, 1.7855\},\\
\Delta^{L}_{1,0} &= \{0.7500, 0.7482, 0.9442, 1.2183, 1.6559\},\\
\Delta^{L}_{2,0} &= \{0.6000, 0.6229, 0.8184, 1.1006, 1.5520\},\\
\Delta^{L}_{3,0} &= \{0.5000, 0.5360, 0.7271, 1.0098, 1.4662\},\\
\Delta^{L}_{4,0} &= \{0.4286, 0.4718, 0.6570, 0.9371, 1.3937\}. \quad (48)
\end{aligned}$$

We can see that the longitudinal piece has a bad convergence in the FOPT scheme. The total contribution of Δ_{kl} is

$$\begin{aligned}
\Delta_{0,0} &= \{1.0000, 0.5410, 0.4761, 0.4610, 0.4586\},\\
\Delta_{1,0} &= \{0.9375, 0.5675, 0.5486, 0.5805, 0.6368\},\\
\Delta_{2,0} &= \{0.9000, 0.5894, 0.6071, 0.6812, 0.7952\},\\
\Delta_{3,0} &= \{0.8750, 0.6082, 0.6565, 0.7694, 0.9393\},\\
\Delta_{4,0} &= \{0.8571, 0.6248, 0.6997, 0.8484, 1.0725\}. \quad (49)
\end{aligned}$$

We can see that the convergence behavior of the dimension-2 contribution in Eq. (49) is not very different from the CIPT scheme in Eq. (43).

C. RGSPT scheme

In optimal renormalization, masses and coupling are fixed at some renormalization scale, but the RG summed running logarithms are evolved around the contour. Interestingly, contour integration can be done analytically, similarly to FOPT. However, due to the summation of the running logarithms, the resulting perturbative contributions are much closer to the CIPT numbers as can be seen later in this subsection.

The perturbative series in the RGSPT scheme for dimension-2 Adler functions has the form

$$\Delta^J_{kl}(x,\xi) = \sum_{i=0}^{4}\sum_{n=0}^{i}\sum_{m=0}^{n} x^i(\xi^2 M_\tau^2)\tilde{T}^J_{i,n,m} K^{kl,J}_{n,m}(x,\xi), \quad (50)$$

which is obtained by inserting Eq. (D11) into Eq. (37), and the corresponding contour integrals $K^{kl,J}_{n,m}(x,\xi)$ have the following form:

$$\begin{aligned}
K^{kl,L+T}_{n,m}(x,\xi) \equiv \frac{-1}{4\pi i}\oint_{|x_c|=1}\frac{dx_c}{x_c^2}\mathcal{F}^{L+T}_{kl}(x_c)\\
\times\frac{\log^n(1-\beta_0 x(\xi^2M_\tau^2)\log(-\xi^2/x_c))}{(1-\beta_0 x(\xi^2M_\tau^2)\log(-\xi^2/x_c))^m}, \quad (51)
\end{aligned}$$

$$\begin{aligned}
K^{kl,L}_{n,m}(x,\xi) \equiv \frac{1}{2\pi i}\oint_{|x_c|=1}\frac{dx_c}{x_c}\mathcal{F}^{L}_{kl}(x_c)\\
\times\frac{\log^n(1-\beta_0 x(\xi^2M_\tau^2)\log(-\xi^2/x_c))}{(1-\beta_0 x(\xi^2M_\tau^2)\log(-\xi^2/x_c))^m}. \quad (52)
\end{aligned}$$

The $\Delta^{L+T}_{i,0}$ contributions for different moments are given by

$$\begin{aligned}
\Delta^{L+T}_{0,0} &= \{0.8878, 0.2307, 0.0799, -0.0328, -0.1561\},\\
\Delta^{L+T}_{1,0} &= \{0.9990, 0.3690, 0.2263, 0.1220, -0.0176\},\\
\Delta^{L+T}_{2,0} &= \{1.0885, 0.4931, 0.3736, 0.2980, 0.1691\},\\
\Delta^{L+T}_{3,0} &= \{1.1652, 0.6095, 0.5246, 0.4957, 0.4043\},\\
\Delta^{L+T}_{4,0} &= \{1.2336, 0.7212, 0.6806, 0.7153, 0.6891\}. \quad (53)
\end{aligned}$$

The $\Delta^L_{i,0}$ have the form

$$\begin{aligned}
\Delta^{L}_{0,0} &= \{1.4048, 1.2210, 1.2280, 1.3899, 1.7560\},\\
\Delta^{L}_{1,0} &= \{1.1360, 1.1034, 1.2194, 1.5005, 2.0514\},\\
\Delta^{L}_{2,0} &= \{0.9687, 1.0302, 1.2287, 1.6169, 2.3536\},\\
\Delta^{L}_{3,0} &= \{0.8538, 0.9808, 1.2477, 1.7375, 2.6655\},\\
\Delta^{L}_{4,0} &= \{0.7697, 0.9459, 1.2727, 1.8617, 2.9888\}, \quad (54)
\end{aligned}$$

and the $\Delta(x)$ behave as

$$\begin{aligned}\Delta_{0,0} &= \{1.0171, 0.4783, 0.3669, 0.3229, 0.3219\},\\ \Delta_{1,0} &= \{1.0332, 0.5526, 0.4746, 0.4666, 0.4996\},\\ \Delta_{2,0} &= \{1.0585, 0.6274, 0.5874, 0.6277, 0.7153\},\\ \Delta_{3,0} &= \{1.0874, 0.7023, 0.7054, 0.8061, 0.9696\},\\ \Delta_{4,0} &= \{1.1176, 0.7774, 0.8286, 1.0019, 1.2640\}. \end{aligned} \tag{55}$$

We can see from the numerical values provided in Eq. (42), (48), and (54) that the longitudinal contributions have a convergence issue, and it is difficult to get reliable determinations using them as input. However, the important ingredient in the mass determination is $\Delta_{i,j}$, defined in Eq. (38). We can see from the numerical values presented in Eqs. (43), (49), and (55) that these inputs can be taken in the mass determination if we truncate the perturbation series to the term which gives the minimum contribution to it. This minimum term of the perturbative series is taken as the truncation uncertainty. This prescription has already been advocated in Ref. [32], and we have termed this procedure of truncation prescription I. Another choice is to use all available terms of the perturbation series coefficients of the Adler function, including the estimate for the unknown $\mathcal{O}(\alpha_s^4)$ term of the $L+T$ component of the dimension-2 Adler function, termed prescription II. These prescriptions have some advantages and disadvantages, which will be discussed later.

VI. PHENOMENOLOGICAL CONTRIBUTION TO THE LONGITUDINAL SECTOR

We can see from the Sec. V that although the contributions from the $L+T$ part of dimension 2 have better convergence for CIPT and RGSPT relative to the FOPT, the longitudinal contributions force us to truncate the higher-order terms. These pathological contributions get enhanced for higher moments and restrict one to use only the leading-order term of the perturbation series. This problem is solved by replacing the longitudinal perturbative series contributions with the phenomenological contributions from chiral perturbation theory [15–19]. These contributions carry significantly less theoretical uncertainty and agree well with the corresponding pQCD results, as shown in Ref. [15]. With these advantages at hand, the strange quark mass determination using the pQCD contribution from the $L+T$ component of the Adler function, combined with phenomenological longitudinal contributions in Sec. VIII, can be performed.

The relevant quantities of interest for phenomenological contributions to $R^{kl,L}_{ij,V/A}$—the longitudinal component of Eq. (7)—are vector/axial-vector spectral functions $\rho^{V/A}_{ij}(s)$. They are related by

$$R^{kl,L}_{ij,V/A} = -24\pi^2 \int_0^1 dx_c (1-x_c)^{2+k} x_c^{l+1} \rho^{V/A,L}_{ij}(M_\tau^2 x_c). \tag{56}$$

The pseudoscalar spectral function receives contributions from pion and kaon mass poles and higher resonances in the strange and nonstrange channels. We use the Maltman and Kambor [16] parametrization of the pseudoscalar spectral function for the us and ud channels in our analysis, which is given by

$$s^2 \rho^{A,L}_{us}(s) = 2 f_K^2 m_K^2 \delta(s - m_K^2) + \sum_{i=1,2} 2 f_i^2 M_i^2 B_i(s). \tag{57}$$

Here f_i and M_i are the decay constants and masses of resonances, and $B_i(s)$ is the Breit-Wigner resonance function taking the form

$$B_i(s) = \frac{1}{\pi} \frac{\Gamma_i M_i}{(s - M_i^2)^2 + \Gamma_i^2 M_i^2}, \tag{58}$$

where Γ_i is the decay width of the resonances. The spectral function for the ud channel is obtained by replacing the kaon terms with the pion in Eq. (57). For the resonance contributions to pseudoscalar ud and us channels appearing in Eq. (57), we use the data in Table III.

The vector component of the spectral function receives dominant contributions from the scalar channels $K\pi$, $K\eta$, and $K\eta'$, and the spectral function has the following form [19]:

$$\rho^{V,L}_{uj}(s) = \frac{3\Delta_{K\pi}^2}{32\pi^2} \sum_{i=\{\pi,\eta,\eta'\}} \sigma_{Ki} |F_{Ki}(s)|^2, \tag{59}$$

where $\Delta_{K\pi} \equiv M_K^2 - M_\pi^2$. The phase space factor $\sigma_{Ki}(s)$ is given by

$$\begin{aligned}\sigma_{Ki}(s) &= \theta(s - (M_K + M_i)^2)\\ &\times \sqrt{\left(1 - \frac{(M_K + M_i)^2}{s}\right)\left(1 + \frac{(M_K - M_i)^2}{s}\right)}. \end{aligned} \tag{60}$$

The strangeness-changing scalar form factors $F_{Ki}(s)$ are defined by

TABLE III. Masses and decay width taken from PDG [33] and decay constants from Ref. [17].

	$\pi(1300)$	$\pi(1800)$	$K(1460)$	$K(1800)$
M_i (MeV)	1300	1810	1482	1830
Γ_i (MeV)	400	215	335	250
f_i (MeV)	2.2 ± 0.46	0.19 ± 0.19	21.4 ± 2.8	4.5 ± 4.5

TABLE IV. Weighted average of the strange quark mass in different perturbative schemes.

	$m_s(M_\tau^2)$ using prescription I (in MeV)		$m_s(M_\tau^2)$ using prescription II (in MeV)	
Perturbative scheme	ALEPH	OPAL	ALEPH	OPAL
CIPT	117.7 ± 28.5	105.9 ± 27.5	93.2 ± 24.1	84.1 ± 22.7
FOPT	129.3 ± 33.5	116.2 ± 29.2	94.2 ± 25.4	85.2 ± 23.9
RGSPT	120.2 ± 23.4	107.7 ± 25.1	89.4 ± 16.4	80.1 ± 15.8

$$\langle \Omega | \partial^\mu (\bar{s}\gamma_\mu u | \Omega \rangle) \equiv -i\sqrt{\frac{3}{2}}\Delta_{K\pi} F_{K\pi}(s) \tag{61}$$

and can be found in Ref. [18]. A detailed discussion on the application of these form factors in the extraction of strange quark mass can be found in Refs. [15,19].

VII. STRANGE QUARK MASS DETERMINATION FROM pQCD

The strange quark mass determination in this section is based on the method used in Refs. [20,22,32]. In addition, we employ different schemes to perform the comparative study. The strange quark mass determination from hadronic τ decays using RGSPT has been performed in Ref. [20]. However, the uncertainties coming from the truncation of perturbative series and the scale dependence of strange quark masses are neglected. We improve the previous determination using pQCD inputs by including these uncertainties and the determinations made in the two prescriptions mentioned in Sec. V.

It should be noted that the higher-dimensional OPE contributions ($d > 4$) to the Adler functions are numerically small [22] and not considered in this analysis. The strange quark mass is determined by supplying experimental and theoretical inputs to Eq. (13). The rhs of the equation is provided with theory inputs from dimension-2 contributions in Eqs. (D5) and (D8) and dimension-4 contributions in Eqs. (33) and (34). These quantities are evaluated along the complex contour in different schemes, as explained in Sec. V. We present our weighted average determinations for $m_s(M_\tau^2)$ from different moments in Table IV for different schemes. The details of various sources of uncertainty in the two prescriptions are presented in Appendix E 1.

We can see from Table IV that the strange quark mass determinations from different schemes agree with each other within uncertainties. It is also evident from the tables presented in Appendix E 1 that the uncertainties in the final strange quark mass are higher in prescription I than in prescription II, mainly due to the truncation of the perturbative series. We also emphasize that the systematic comparison of the behavior of the perturbative series in different schemes can only be made in prescription II, where the same order information is used. RGSPT provides better control over the theoretical uncertainty by minimizing the renormalization scale dependence. The scale dependence of the strange quark mass for various moments is shown in Fig. 1, plotted using prescription II. These plots indicate that the strange mass from the RGSPT scheme is stable for a wider range of scale variations for the moments under consideration. It should be noted that the uncertainties associated with renormalization scale dependence are included only in the range $\xi \in [0.75, 2.0]$ in the strange mass determination in Table IV.

It should be noted that the poor convergence of the longitudinal contributions restricts this method to be applicable in the lower energies $s_0 < M_\tau^2$. Additional uncertainties in the determination of m_s arise due to the variations of the upper limit of the moment in the integral s_0 defined in Eq. (4). These are estimated using the phenomenological determination, discussed in the next section, and are also included in Table IV. Further details on the numerical uncertainties using pQCD inputs can be found in Appendix E 1.

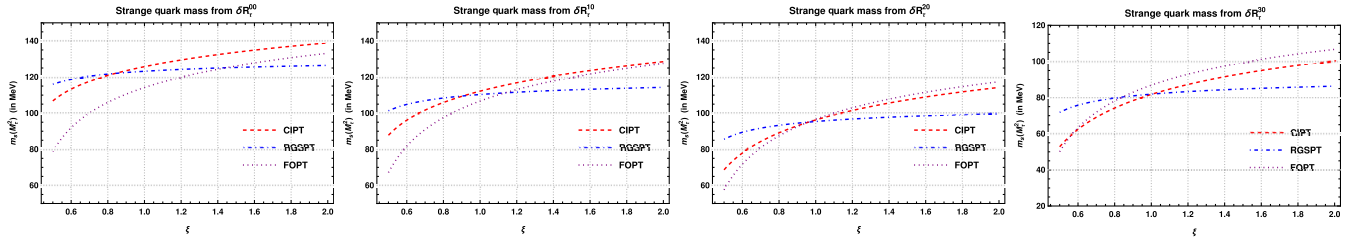

FIG. 1. Scale variation of the strange quark mass in different perturbative schemes using pQCD inputs.

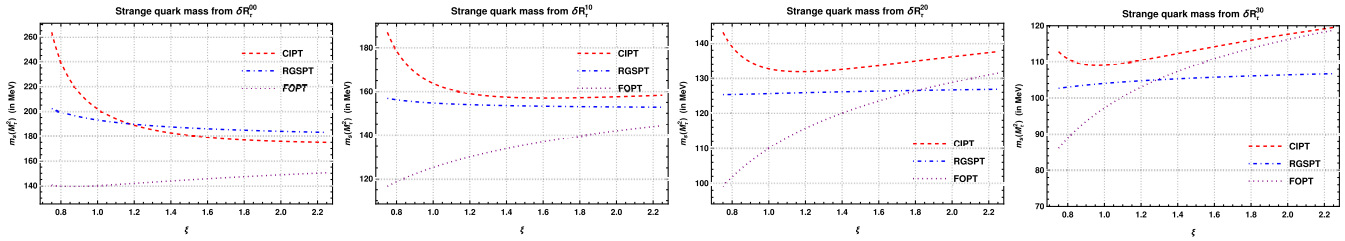

FIG. 2. Scale variation of the strange quark mass obtained from phenomenological inputs in different perturbative schemes.

VIII. STRANGE QUARK MASS DETERMINATION USING PHENOMENOLOGICAL INPUT

The determination of the strange quark mass in this section is similar to the one used in Sec. VII, but now the longitudinal Adler function is replaced with the phenomenologically parametrized contributions, as discussed in Sec. VI. It should be noted that the $L+T$ component of the Adler function at dimension 2 is known to $\mathcal{O}(\alpha_s^3)$, and we do not use its estimate for the $\mathcal{O}(\alpha_s^4)$ coefficient in the determination of $m_s(M_\tau^2)$ using phenomenological inputs. Contributions from the last known term of the perturbation series of the Adler function are taken as the total truncation uncertainty, similar to that of the previous section.

Following the discussion of Sec. VI, we now have all the necessary ingredients for the strange quark mass determination. Using the transverse contributions from Sec. VII and combining them with the input from Sec. VI, we determine the strange quark in different schemes. We present our result for the weighted average in Table V, and further details of the determinations from the moments can be found in Appendix E 2. The scale dependence in $m_s(M_\tau^2)$ is presented in Fig. 2 using prescription II. As observed in the previous section, the strange quark mass determinations from the RGSPT scheme are stable over the wider range of scale variation for the moments under consideration. The determination of m_s from the traditional spectral moments is sensitive to the variation of s_0. A typical 5% variation of s_0 from M_τ^2 in the range $s_0 \in [3, M_\tau^2]$ induces variations of about 6%–13% in the m_s determinations from the moments using the OPAL data. Unfortunately, such variations cannot be calculated for the ALEPH moments as the strange spectral function is not publicly available. These uncertainties are estimated from the determinations using the OPAL data.

IX. DETERMINATION OF $|V_{us}|$

The data on strange and nonstrange spectral moments for the hadronic τ decay provided by ALEPH [26,63,64], HFLAV [65], and OPAL [27] collaborations can be used to determine the CKM matrix element $|V_{us}|$. These experimental moments, along with the theoretical moments calculated with strange quark mass as input from other sources, can be used to determine $|V_{us}|$ applying the following relation:

$$|V_{us}| = \sqrt{\frac{R_{\tau,S}^{kl}}{R_{\tau,V+A}^{kl}/|V_{ud}|^2 - \delta R_{\tau,th}^{kl}}}, \tag{62}$$

where $R_{\tau,S}^{kl}$ and $R_{\tau,V+A}^{kl}$ are experimental inputs and $\delta R_{\tau,th}^{kl}$ is the theory input, in which $m_s(2\ \mathrm{GeV})$ is taken as an external input. This method has already been used previously in Refs. [15,66–70], and it has been observed that the uncertainties are dominated by the experimental data available for the strange component. An additional source of uncertainties is pointed out in Ref. [66] due to s_0 variations, which can be solved using a different analysis based on the nonspectral weight functions. However, we restrict this analysis to only the traditional weight functions.

Using $m_s(2\ \mathrm{GeV}) = 93 \pm 11\ \mathrm{MeV}$ [33] as an external input and ALEPH data [26,63,64], we present our determination for $|V_{us}|$ in Table VI.

The latest branching fraction of hadronic τ decays into nonstrange and slightly more precise strange components from HFLAV [65] can also be used to get a more precise determination of $|V_{us}|$ from this method. The results for different schemes are presented in Table VII.

The uncertainties shown in these tables are dominated by those coming from the variation of $s_0 \in [2.5, M_\tau^2]$ and

TABLE V. Weighted average of strange quark mass in the different perturbative schemes. Phenomenological inputs for the longitudinal contributions are used.

	$m_s(M_\tau^2)$ using prescription I (in MeV)		$m_s(M_\tau^2)$ using prescription II (in MeV)	
Perturbative scheme	ALEPH	OPAL	ALEPH	OPAL
CIPT	123.3 ± 22.3	106.3 ± 21.5	125.1 ± 25.1	107.5 ± 23.9
FOPT	136.6 ± 35.0	119.5 ± 35.4	115.8 ± 30.1	101.6 ± 28.3
RGSPT	123.1 ± 21.1	107.0 ± 21.2	117.7 ± 20.1	102.0 ± 19.5

TABLE VI. $|V_{us}|$ from ALEPH data in different perturbative schemes using $\delta R^{kl}_{\tau,th}$ from Secs. VII and VIII.

	$\lvert V_{us}\rvert$	
Scheme	pQCD inputs	Phenomenological inputs
CIPT	0.2174 ± 0.0045	0.2168 ± 0.0044
FOPT	0.2183 ± 0.0055	0.2179 ± 0.0055
RGSPT	0.2178 ± 0.0046	0.2170 ± 0.0045

TABLE VII. $|V_{us}|$ from HFLAV data in different perturbative schemes using $\delta R^{kl}_{\tau,th}$ from Secs. VII and VIII.

	$\lvert V_{us}\rvert$	
Scheme	pQCD inputs	Phenomenological inputs
CIPT	0.2195 ± 0.0047	0.2189 ± 0.0044
FOPT	0.2205 ± 0.0043	0.2200 ± 0.0037
RGSPT	0.2199 ± 0.0046	0.2191 ± 0.0043

experimental uncertainties in strange $R_{\tau,S}$ contributions. It should be noted that uncertainties coming from the variation of s_0 in Tables VI and VII are calculated using the experimental data on the spectral function from Refs. [26,27].

The $|V_{us}|$ determinations from ALEPH [26,63,64] and HFLAV [65] are based on the (0, 0) moment. A detailed analysis for higher moments can be performed using the OPAL [27] data, where $(k, 0)$ moments for $k = 0, \ldots, 4$ are also available. These moments are correlated, and their correlation should also be considered in the full analysis. Given the large uncertainties in their strange components and unknown precise higher-dimensional OPE corrections, we neglect these correlations among various moments in our determinations from these data.

Using the strange and nonstrange moments from OPAL and the theoretical inputs for $\delta R^{kl}_{\tau,th}$ from Sec. VII, we present the weighted average of the determination $|V_{us}|$ from prescriptions I and II in Table VIII. Details of the $|V_{us}|$ from the moments along with the sources of uncertainties can be found in Tables XX and XXI, respectively. We can observe from these tables that the RGSPT is slightly more sensitive to the strange quark mass taken as input, but the overall theory uncertainty coming into this scheme is less than CIPT and FOPT in prescription II. We can also see that the divergent nature of the longitudinal component is still an issue, causing a large theoretical uncertainty dominating in the higher moments in prescription II in Table XXI.

TABLE IX. Joint determination of $m_s(2\ \text{GeV})$ and $|V_{us}|$ from OPAL data with moment $(k, 0)$ with $k = 0, 1, 2, 3, 4$ in different perturbative schemes using pQCD inputs as well as phenomenological inputs.

	Phenomenological inputs			
	Prescription I		Prescription II	
Scheme	$m_s(2\ \text{MeV})$	$\lvert V_{us}\rvert$	$m_s(2\ \text{MeV})$	$\lvert V_{us}\rvert$
CIPT	75	0.2199	75	0.2199
FOPT	46	0.2227	46	0.2227
RGSPT	73	0.2199	73	0.2199

These shortcomings are slightly improved in the phenomenological determination and can be seen in Tables XXII and XXIII. Again, these determinations suffer from large s_0 and theoretical uncertainties, especially those coming from the strange quark mass in the higher moments. It is worth emphasizing that prescription I reduces the dependence on the spectral moments in the $|V_{us}|$ determination. The weighted averages of these results for $|V_{us}|$ are presented in Table VIII. The RGSPT scheme is slightly more sensitive to the variation of s_0, which, compared to CIPT, dominates in the final average presented in Table XXII and can be seen in the table presented in Appendix E 3.

X. JOINT m_s AND $|V_{us}|$ DETERMINATION

The experimental moments provided by the OPAL Collaboration in Ref. [27] can be used for the joint extraction of m_s and $|V_{us}|$. It should be noted that the moments provided in Ref. [27] are correlated, and a proper analysis will require their correlations to be taken into account. Given the uncertainties present in the data, we disregard these correlations and restrict ourselves to a simplified analysis.

Using the phenomenological parametrization for the longitudinal contributions and the perturbative $L + T$ component from Secs. VI and IV, we fit the $m_s(2\ \text{GeV})$ and $|V_{us}|$ to Eq. (62) for moments $(k, 0)$ with $k = 0, 1, \ldots, 4$.

TABLE VIII. Weighted average of the determination of $|V_{us}|$ from the OPAL data in different perturbative schemes.

	$\lvert V_{us}\rvert$ from prescription I		$\lvert V_{us}\rvert$ from prescription II	
Perturbative scheme	pQCD inputs	Phenomenological inputs	pQCD inputs	Phenomenological inputs
CIPT	0.2220 ± 0.0050	0.2212 ± 0.0047	0.2232 ± 0.0048	0.2212 ± 0.0045
FOPT	0.2212 ± 0.0059	0.2220 ± 0.0054	0.2240 ± 0.0059	0.2224 ± 0.0054
RGSPT	0.2222 ± 0.0051	0.2215 ± 0.0048	0.2238 ± 0.0049	0.2215 ± 0.0047

The central values of the joint fit are presented in Table IX. These joint fits give smaller values for $m_s(2\ \mathrm{GeV})$ and $|V_{us}|$ compared to the PDG average [33], but they are very close to the findings of Gamiz *et al.* [67] for CIPT and RGSPT.

XI. SUMMARY AND CONCLUSION

The hadronic τ decays are important ingredients for extracting various QCD parameters. We have used perturbative schemes CIPT, FOPT, and RGSPT in the extraction of m_s, $|V_{us}|$, and their joint determinations from the experimental inputs available from ALEPH [26,63,64], HFLAV [65], and OPAL [27] moments of hadronic τ decays. To reach the goal, we first calculate the RGSPT coefficients for the dimension-4 operator and use them for the determination of m_s and $|V_{us}|$. Dimension-6 OPE corrections are known to NLO, and their RG improvement is discussed in Refs. [71–73]. Four quark condensates present in these contributions are estimated using the vacuum saturation approximation [74]; they are found to be numerically very small and are not considered in this article. Higher-dimensional OPE corrections are not fully known and are neglected in this article.

The moments calculated using perturbation theory suffer from convergence issues, so we have employed two prescriptions. The central values of the strange quark mass determinations from prescription I are less spread out for different moments than in prescription II. The theoretical uncertainties arising from truncation and scale dependence dominate for higher moments in prescription I for CIPT and FOPT. However, RGSPT has better control over the scale dependence for a wider range of scale variation, even for higher moments as shown in Figs. 1 and 2. This improvement results in a more precise determination in RGSPT compared to FOPT and CIPT schemes.

The important results of this article for the $m_s(M_\tau^2)$ determination are presented in Tables IV and V and for $|V_{us}|$ determinations in Tables VI–VIII. The joint m_s and $|V_{us}|$ determination results are presented in Table IX. It should be noted that the ALEPH moments used in the m_s determinations in this article are based on the old $|V_{us}|$ calculated in Ref. [32]. The strange quark mass determinations from the moments are very sensitive to the value of $|V_{us}|$, and hence we do not consider them in the final average. However, the experimental data for the strange and nonstrange moments provided by the OPAL Collaboration in Ref. [27], with the current value of $|V_{us}| = 0.2245 \pm 0.0008$ [33] as an input, can be used to provide the most updated determination of the strange quark mass.

We give our final determination for $m_s(M_\tau^2)$, which comes from the weighted average of strange quark mass determinations using the RGSPT scheme from Table V:

$$m_s(M_\tau^2) = 102.0 \pm 19.5\ \mathrm{MeV} \quad (\mathrm{OPAL, RGSPT}), \tag{63}$$

which corresponds to the strange quark mass at 2 GeV:

$$m_s(2\ \mathrm{GeV}) = 98 \pm 19\ \mathrm{MeV}. \tag{64}$$

Using ALEPH [26,64] moments, the $|V_{us}|$ determinations along with their deviation from PDG [33] ($|V_{us}| = 0.2243 \pm 0.0008$) and the CKM unitarity fit value ($|V_{us}| = 0.2277 \pm 0.0013$) are

$$|V_{us}| = 0.2168 \pm 0.0044 \quad (1.7\sigma, 2.6\sigma) \quad (\text{for CIPT}), \tag{65}$$

$$|V_{us}| = 0.2170 \pm 0.0045 \quad (1.6\sigma, 2.3\sigma) \quad (\text{for RGSPT}), \tag{66}$$

and from HFLAV [65],

$$|V_{us}| = 0.2189 \pm 0.0044 \quad (1.2\sigma, 1.9\sigma) \quad (\text{for CIPT}), \tag{67}$$

$$|V_{us}| = 0.2191 \pm 0.0043 \quad (1.2\sigma, 1.9\sigma) \quad (\text{for RGSPT}). \tag{68}$$

The weighted average of the $|V_{us}|$ determinations from OPAL [27] using phenomenological inputs is presented in Table VIII. The most precise determinations for $|V_{us}|$ from this table come from CIPT and RGSPT:

$$|V_{us}| = 0.2212 \pm 0.0047,\ \ 0.2212 \pm 0.0045 \quad (\text{for CIPT}), \tag{69}$$

$$|V_{us}| = 0.2215 \pm 0.0048,\ \ 0.2215 \pm 0.0047 \quad (\text{for RGSPT}). \tag{70}$$

The mean values of the determinations in these schemes are

$$|V_{us}| = 0.2212 \pm 0.0045 \quad (0.7\sigma, 1.4\sigma) \quad (\text{for CIPT}), \tag{71}$$

$$|V_{us}| = 0.2215 \pm 0.0047 \quad (0.6\sigma, 1.3\sigma) \quad (\text{for RGSPT}). \tag{72}$$

We give our final determinations by the weighted average of these results as

$$|V_{us}| = 0.2189 \pm 0.0044 \quad (1.2\sigma, 1.9\sigma) \quad (\text{for CIPT}), \tag{73}$$

$$|V_{us}| = 0.2191 \pm 0.0043 \quad (1.2\sigma, 1.9\sigma) \quad (\text{for RGSPT}). \tag{74}$$

The values obtained for $|V_{us}|$ using OPAL data agree with the PDG average within uncertainties. However, the $|V_{us}|$ determination from ALEPH [26,63,64] and HFLAV [65] are more than 1.2σ and 1.9σ away from the PDG [33] average and CKM unitarity fit value. It should be noted that the PDG average is already in tension with 2.2σ with the CKM unitarity.

The dependence of our determinations on the choice of the moments and their correlation is not considered in this article, and we expect that these can be further improved using nonspectral weights employed by Maltman *et al.* in Refs. [75–77].

ACKNOWLEDGMENTS

We thank Professor Diogo Boito for providing help with the experimental data on the spectral functions. D. D. would like to thank the Department of Science and Technology, Government of India for the INSPIRE Faculty Award (Grant No. IFA16-PH170). D. D. also thanks the Institute for Theoretical Physics III, University of Stuttgart for kind hospitality during various stages of the work. A. K. thanks Shiuli Chatterjee, Rhitaja Sengupta, and Prasad Hegde for their valuable discussions. A. K. is supported by a fellowship from the Ministry of Human Resources Development, Government of India.

APPENDIX A: RUNNING OF THE STRONG COUPLING AND QUARK MASSES IN pQCD

The running of strong coupling and the quark masses is computed by solving the following differential equations:

$$\mu^2\frac{d}{d\mu^2}x(\mu^2)=\beta(x(\mu^2))=-\sum_i x^{i+2}(\mu^2)\beta_i,\qquad \mu^2\frac{d}{d\mu^2}m_i(\mu^2)\equiv m_i(\mu^2)\gamma_m=-m_i(\mu^2)\sum_i\gamma_i x^{i+1}(\mu^2). \tag{A1}$$

The series solutions for the running of strong coupling and the quark masses relevant for contour integration in the complex plane using FOPT are

$$\begin{aligned}x(q^2)=x\Bigg\{&1+x\beta_0L+x^2(\beta_1L+\beta_0^2L^2)+x^3\left(\beta_2L+\frac{5}{2}\beta_1\beta_0L^2+\beta_0^3L^3\right)\\&+x^4\left(\beta_3L+\left(\frac{3\beta_1^2}{2}+3\beta_0\beta_2\right)L^2+\frac{13}{3}\beta_1\beta_0^2L^3+\beta_0^4L^4\right)\\&+x^5\left(\beta_4L+\left(\frac{7\beta_1\beta_2}{2}+\frac{7\beta_0\beta_3}{2}\right)L^2+\left(6\beta_2\beta_0^2+\frac{35}{6}\beta_1^2\beta_0\right)L^3+\frac{77}{12}\beta_1\beta_0^3L^4+\beta_0^5L^5\right)\Bigg\}+\mathcal{O}(\alpha_s^7),\end{aligned} \tag{A2}$$

$$\begin{aligned}m_i(q^2)=m0_i\Bigg\{&1+x\gamma_0L+x^2\left(\gamma_1L+\frac{1}{2}\gamma_0L^2(\beta_0+\gamma_0)\right)\\&+x^3\left(\gamma_2L+L^2\left(\frac{\beta_1\gamma_0}{2}+\gamma_1(\beta_0+\gamma_0)\right)+\frac{1}{6}\gamma_0L^3(\beta_0+\gamma_0)(2\beta_0+\gamma_0)\right)\\&+x^4\Bigg(\gamma_3L+L^2\left(\beta_1\gamma_1+\frac{\beta_2\gamma_0}{2}+\frac{3\beta_0\gamma_2}{2}+\frac{\gamma_1^2}{2}+\gamma_0\gamma_2\right)+\frac{1}{24}\gamma_0L^4(\beta_0+\gamma_0)(2\beta_0+\gamma_0)(3\beta_0+\gamma_0)\\&+L^3\left(\frac{1}{6}(\beta_1\gamma_0(5\beta_0+3\gamma_0)+3\gamma_1(\beta_0+\gamma_0)(2\beta_0+\gamma_0))\right)\Bigg)\\&+x^5\Bigg(\gamma_4L+\frac{1}{2}L^2(\beta_3\gamma_0+3\beta_1\gamma_2+2\gamma_1(\beta_2+\gamma_2)+2\gamma_3(2\beta_0+\gamma_0))\\&+\frac{1}{6}L^3(3\beta_1^2\gamma_0+\beta_1\gamma_1(14\beta_0+9\gamma_0)+3(2\beta_0+\gamma_0)(\beta_2\gamma_0+\gamma_2(2\beta_0+\gamma_0)+\gamma_1^2))\\&+\frac{1}{12}L^4(\beta_1\gamma_0(13\beta_0\gamma_0+13\beta_0^2+3\gamma_0^2)+2\gamma_1(\beta_0+\gamma_0)(2\beta_0+\gamma_0)(3\beta_0+\gamma_0))\\&+\frac{1}{120}\gamma_0L^5(\beta_0+\gamma_0)(2\beta_0+\gamma_0)(3\beta_0+\gamma_0)(4\beta_0+\gamma_0)\Bigg)\Bigg\}+\mathcal{O}(\alpha_s^6),\end{aligned} \tag{A3}$$

where $x\equiv x(\mu^2)$, $L=\log(\mu^2/q^2)$, β_i are the QCD beta function coefficients, and γ_i are the coefficients of the anomalous dimension of the quark mass.

The QCD beta function coefficients are known to five loops [78–86], and their analytic expressions for the active flavor $n_f = 3$ are

$$\beta_0 = 9/4, \qquad \beta_1 = 4, \qquad \beta_2 = 3863/384, \qquad \beta_3 = 140599/4608 + (445\zeta(3))/32,$$
$$\beta_4 = \frac{11059213\zeta(3)}{55296} - \frac{534385\zeta(5)}{3072} - \frac{801\pi^4}{2048} + \frac{139857733}{1327104}. \tag{A4}$$

The known five-loop quark mass anomalous dimension coefficients [87–94] for $n_f = 3$ are

$$\gamma_m^{(0)} = 1, \qquad \gamma_m^{(1)} = \frac{91}{24}, \qquad \gamma_m^{(2)} = \frac{8885}{576} - \frac{5\zeta(3)}{2}, \qquad \gamma_m^{(3)} = -\frac{9295\zeta(3)}{432} - \frac{125\zeta(5)}{12} + \frac{3\pi^4}{32} + \frac{2977517}{41472},$$
$$\gamma_m^{(4)} = \frac{156509815}{497664} - \frac{23663747\zeta(3)}{124416} + 85\zeta(3)^2 + \frac{4753\pi^4}{4608} + \frac{118405\zeta(7)}{576} - \frac{22625465\zeta(5)}{62208} + \frac{125\pi^6}{2016}. \tag{A5}$$

We also need the vacuum anomalous dimension for dimension-4 operators, which has recently been computed to five loops [95]. Their analytic expression of the diagonal component relevant for this article is given by

$$\begin{aligned}\hat{\gamma}_0^{di} &\equiv \frac{3}{16\pi^2}\gamma_n^{ii}x^n \\ &= \frac{3}{16\pi^2}\left\{-1 - \frac{4x}{3} + x^2\left(\frac{2\zeta(3)}{3} - \frac{223}{72}\right) + x^3\left(\frac{346\zeta(3)}{9} - \frac{1975\zeta(5)}{54} + \frac{13\pi^4}{540} - \frac{3305}{1296}\right)\right. \\ &\quad \left. + x^4\left(\frac{6121\zeta(3)^2}{864} - \frac{11881\pi^4}{8640} + \frac{1680599\zeta(3)}{2592} + \frac{36001\zeta(7)}{96} + \frac{93925\pi^6}{326592} - \frac{59711\zeta(5)}{48} + \frac{16141627}{248832}\right)\right\}.\end{aligned} \tag{A6}$$

APPENDIX B: RGSPT COEFFICIENTS RELEVANT FOR THE DIMENSION-0 AND DIMENSION-2 ADLER FUNCTIONS

The first three summed series coefficients are presented as

$$S_0[w] = w^{-n_2\tilde{\gamma}_0 - n_1}, \tag{B1}$$

$$S_1[w] = w^{-n_2\tilde{\gamma}_0 - n_1 - 1}(T_{1,0} - n_1\tilde{\beta}_1 L_w + n_2 \times (-\tilde{\beta}_1\tilde{\gamma}_0 + \tilde{\gamma}_1 + w\tilde{\beta}_1\tilde{\gamma}_0 - \tilde{\beta}_1\tilde{\gamma}_0 L_w - w\tilde{\gamma}_1)), \tag{B2}$$

$$\begin{aligned}S_2[w] = w^{-n_2\tilde{\gamma}_0 - n_1 - 2}&\left\{T_{2,0} + T_{1,0}(n_2(\tilde{\gamma}_1 - \tilde{\beta}_1\tilde{\gamma}_0) + n_2 w(\tilde{\beta}_1\tilde{\gamma}_0 - \tilde{\gamma}_1) + L_w(-n_2\tilde{\beta}_1\tilde{\gamma}_0 - n_1\tilde{\beta}_1 - \tilde{\beta}_1))\right. \\ &+ \left\{n_1(\tilde{\beta}_2 - \tilde{\beta}_1^2) + n_2\left(-\frac{1}{2}\tilde{\beta}_1^2\tilde{\gamma}_0 - \frac{1}{2}\tilde{\beta}_1\tilde{\gamma}_1 + \frac{1}{2}\tilde{\beta}_2\tilde{\gamma}_0 + \frac{\tilde{\gamma}_2}{2}\right) + w[n_1(\tilde{\beta}_1^2 - \tilde{\beta}_2) + n_2(\tilde{\beta}_1^2\tilde{\gamma}_0 - \tilde{\beta}_2\tilde{\gamma}_0)\right. \\ &+ n_2^2(-\tilde{\beta}_1^2\tilde{\gamma}_0^2 + 2\tilde{\beta}_1\tilde{\gamma}_1\tilde{\gamma}_0 - \tilde{\gamma}_1^2) + L_w(n_2^2(\tilde{\beta}_1\tilde{\gamma}_0\tilde{\gamma}_1 - \tilde{\beta}_1^2\tilde{\gamma}_0^2) + n_1 n_2(\tilde{\beta}_1\tilde{\gamma}_1 - \tilde{\beta}_1^2\tilde{\gamma}_0))] \\ &+ L_w^2\left[\frac{1}{2}n_2^2\tilde{\beta}_1^2\tilde{\gamma}_0^2 + \frac{1}{2}n_1^2\tilde{\beta}_1^2 + \frac{1}{2}n_2\tilde{\beta}_1^2\tilde{\gamma}_0 + n_1\left(n_2\tilde{\beta}_1^2\tilde{\gamma}_0 + \frac{\tilde{\beta}_1^2}{2}\right)\right] + w^2\left[n_2^2\left(\frac{1}{2}\tilde{\beta}_1^2\tilde{\gamma}_0^2 - \tilde{\beta}_1\tilde{\gamma}_1\tilde{\gamma}_0 + \frac{\tilde{\gamma}_1^2}{2}\right)\right. \\ &\left.\left.\left. + n_2\left(-\frac{1}{2}\tilde{\beta}_1^2\tilde{\gamma}_0 + \frac{1}{2}\tilde{\beta}_1\tilde{\gamma}_1 + \frac{1}{2}\tilde{\beta}_2\tilde{\gamma}_0 - \frac{\tilde{\gamma}_2}{2}\right)\right]\right\}\right\},\end{aligned} \tag{B3}$$

where $\tilde{X}_i \equiv X_i/\beta_0$, and the rest can be found by solving Eq. (20) with the boundary condition $S_i[1] = T_{i,0}$, and for simplification of the expressions, we have taken $T_{0,0} = 1$.

APPENDIX C: PERTURBATIVE COEFFICIENTS RELEVANT FOR THE DIMENSION-4 CORRECTIONS AND THEIR RGSPT COEFFICIENTS

The RG-inaccessible coefficients needed for the dimension-4 operators are calculated in Refs. [10,52,58,96–103], and their values are

$$p0_0=0,\quad p0_1=1,\quad p0_2=7/6,\quad q0_0=1,\quad q0_1=-1,\quad q0_2=-131/24,\quad hl0_0=1,\quad kl0_0=1$$
$$t0_0=0,\quad t0_1=1,\quad t0_2=17/2,\quad h0_0=1,\quad g0_0=1,\quad g0_1=94/9-4/3\zeta_3,\quad k0_0=0,\quad k0_1=1. \tag{C1}$$

Perturbative coefficients involving the condensate terms described in Sec. IV C are

$$p_0^{L+T}(w)=0,\qquad p_1^{L+T}(w)=p0_1,\qquad p_2^{L+T}(w)=\frac{\beta_1 p0_1}{\beta_0}+\frac{p0_2-\frac{\beta_1 p0_1}{\beta_0}}{w},$$
$$r_0^{L+T}(w)=0,\qquad r_1^{L+T}(w)=\frac{\gamma_0 p0_1}{6\beta_0 w}-\frac{\gamma_0 p0_1}{6\beta_0},\qquad r_2^{L+T}(w)=\frac{\frac{\beta_1\gamma_0 p0_1}{6\beta_0^2}-\frac{\gamma_0 p0_2}{6\beta_0}}{w},$$
$$q_0^{L+T}(w)=q0_0,\qquad q_1^{L+T}(w)=\frac{q0_1}{w},\qquad q_2^{L+T}(w)=\frac{q0_2-\frac{\beta_1 q0_1\log(w)}{\beta_0}}{w^2},$$
$$t_0^{L+T}(w)=0,\qquad t_1^{L+T}(w)=\frac{t0_1}{w},\qquad t_2^{L+T}(w)=\frac{t0_2-\frac{\beta_1 t0_1\log(w)}{\beta_0}}{w^2}. \tag{C2}$$

The RGSPT coefficients for the coefficients of m^4 to $\mathcal{O}(\alpha_s)$ are

$$k_0^{L+T}(w)=\frac{\gamma_0^{ii} t0_1(2(1-w)w^{-\frac{4\gamma_0}{\beta_0}}-2w^{-\frac{4\gamma_0}{\beta_0}}+2)}{10w(24\gamma_0-2\beta_0)},\qquad g_0^{L+T}(w)=g0_0 w^{-\frac{4\gamma_0}{\beta_0}},\qquad j_0^L(w)=0,\qquad j_1^L(w)=0, \tag{C3}$$

$$k_1^{L+T}(w)=\frac{\gamma_0^{ii} w^{-\frac{4\gamma_0}{\beta_0}-2}}{10\beta_0(\beta_0-4\gamma_0)^2}\left(\beta_1 t0_1\left(w^{\frac{4\gamma_0}{\beta_0}}(\beta_0(\log(w)+1)-4\gamma_0\log(w))-\beta_0 w\right)-\beta_0 t0_2(\beta_0-4\gamma_0)\left(w^{\frac{4\gamma_0}{\beta_0}}-w\right)\right)$$
$$+k0_1 w^{-\frac{4\gamma_0}{\beta_0}-1}+\frac{\frac{\gamma_1^{ii} t0_1}{w}-\gamma_1^{ii} t0_1 w^{-\frac{4\gamma_0}{\beta_0}-1}}{104\gamma_0}, \tag{C4}$$

$$h_0^{L+T}(w)=h0_0 w^{-\frac{4\gamma_0}{\beta_0}}+\frac{q0_1(\frac{1}{w}-w^{-\frac{4\gamma_0}{\beta_0}})}{2(\beta_0-4\gamma_0)}-\frac{q0_0\gamma_1 w^{-\frac{4\gamma_0}{\beta_0}}(\beta_0(w^{\frac{4\gamma_0}{\beta_0}}-1)-4\gamma_0(w-1))}{2\beta_0\gamma_0(\beta_0-4\gamma_0)}$$
$$\times\frac{q0_0 w^{-\frac{4\gamma_0}{\beta_0}}(\beta_0^2(-4\beta_0+3\beta_1+16\gamma_0)(w^{\frac{4\gamma_0}{\beta_0}}-1)+12\beta_1\gamma_0(4\gamma_0(-w+\log(w)+1)-\beta_0\log(w)))}{24\beta_0^2\gamma_0(\beta_0-4\gamma_0)}, \tag{C5}$$

$$h_1^{L+T}(w)=w^{-\frac{4\gamma_0}{\beta_0}-1}\left(\frac{h0_0(4\beta_0\gamma_1-4\beta_1\gamma_0(\log(w)+1))}{\beta_0^2}+h0_1+\frac{\beta_1 q0_0\log(w)(3\beta_1\gamma_0(\log(w)+2)-2\beta_0(\beta_0+3\gamma_1))}{3\beta_0^4}\right)$$
$$+\frac{q0_0(\beta_0^3(-4\beta_1+16\gamma_1+6\gamma_2)+2\beta_0^2(3(\beta_2\gamma_0+4\gamma_1^2)-\beta_1(8\gamma_0+9\gamma_1))+6\beta_1\beta_0\gamma_0(\beta_1-8\gamma_1))w^{-\frac{4\gamma_0}{\beta_0}-1}}{6\beta_0^4(\beta_0+4\gamma_0)}$$
$$+\frac{q0_0(3\beta_2\gamma_0+\gamma_1(4\beta_0-3\beta_1-16\gamma_0+12\gamma_1)-12\gamma_2\gamma_0)}{6\gamma_0(\beta_0^2-16\gamma_0^2)}+\frac{\gamma_2^{ii} q0_0}{2(\beta_0-4\gamma_0)}-\frac{q0_0(\gamma_2^{ii}-8\frac{\beta_1^2\gamma_0^2}{\beta_0^4})w^{-\frac{4\gamma_0}{\beta_0}-1}}{2(\beta_0+4\gamma_0)}$$
$$+\frac{1}{(\beta_0-4\gamma_0)}\left\{\frac{q0_0(\beta_0^3\gamma_2-\beta_0^2(\beta_2\gamma_0+\gamma_1(\beta_1+4\gamma_1))+\beta_1\beta_0\gamma_0(\beta_1+8\gamma_1)-4\beta_1^2\gamma_0^2)w^{1-\frac{4\gamma_0}{\beta_0}}}{\beta_0^4}\right.$$
$$+\frac{\frac{q0_1(-4\beta_0+3\beta_1+16\gamma_0-12\gamma_1)}{24\gamma_0}+w^{-\frac{4\gamma_0}{\beta_0}}(q0_1(\frac{\beta_0}{6\gamma_0}-\frac{\beta_1-4\gamma_1}{8\gamma_0}-\frac{2\gamma_1}{\beta_0}+\frac{2\beta_1\gamma_0(\log(w)+1)}{\beta_0^2}-\frac{2}{3})-\frac{q0_2}{2})}{w}$$
$$\left.+\frac{\frac{q0_2}{2}-\frac{\beta_1 q0_1\log(w)}{2\beta_0}}{w^2}+\frac{2q0_1(\beta_0\gamma_1-\beta_1\gamma_0)w^{-\frac{4\gamma_0}{\beta_0}}}{\beta_0^2}\right\}, \tag{C6}$$

$$g_1^{L+T}(w) = -\frac{\beta_1 4\gamma_0 g0_0 \log(w) w^{-\frac{4\gamma_0}{\beta_0}-1}}{\beta_0^2} + \frac{w^{-\frac{4\gamma_0}{\beta_0}-1}(4\beta_0^2 g0_1 + 4\beta_0\gamma_1 g0_0(1-w) - 4\beta_1 4\gamma_0 g0_0(1-w))}{4\beta_0^2} \tag{C7}$$

$$\begin{aligned} h_0^L(w) = &-\frac{\gamma_0^{ii} w^{-\frac{4\gamma_0}{\beta_0}}(\beta_0^2(\beta_1-\gamma_1)(w^{\frac{4\gamma_0}{\beta_0}}-1) - \beta_0 4\gamma_0(\beta_1\log(w) - \gamma_1(w-1)) + \beta_1 4\gamma_0^2(-w+\log(w)+1))}{8\beta_0^2 4\gamma_0(\beta_0-4\gamma_0)} \\ &+ hl0_0 w^{-\frac{4\gamma_0}{\beta_0}} + \frac{\gamma_1^{ii}(1-w^{-\frac{4\gamma_0}{\beta_0}})}{84\gamma_0} - \frac{\gamma_0^{ii}(1-w^{1-\frac{4\gamma_0}{\beta_0}})}{8x(\beta_0-4\gamma_0)}, \end{aligned} \tag{C8}$$

$$\begin{aligned} h_1^L(w) = &\, w^{-\frac{4\gamma_0}{\beta_0}}\left(-\frac{2\beta_1^2\gamma_0}{\beta_0^4} + \frac{4\beta_1\gamma_1}{\beta_0^3} + \frac{\beta_1\gamma_1}{2\beta_0^2\gamma_0} - \frac{2\gamma_1}{3\beta_0\gamma_0} - \frac{2\gamma_1^2}{\beta_0^2\gamma_0} + \frac{2\beta_1}{3\beta_0^2} - \frac{\beta_2}{2\beta_0^2} + hl0_0\left(\frac{4\beta_1\gamma_0}{\beta_0^2} - \frac{4\gamma_1}{\beta_0}\right) + \frac{\frac{2\gamma_1}{3\gamma_0} + \frac{\gamma_2^{ii}}{2}}{(\beta_0+4\gamma_0)}\right. \\ &\left. + \left(\frac{2\beta_1\gamma_1}{\beta_0^3} - \frac{2\beta_1^2\gamma_0}{\beta_0^4}\right)\log(w)\right) + \frac{(\beta_0^3\gamma_2 - \beta_0^2(\beta_2\gamma_0 + \gamma_1(\beta_1+4\gamma_1)) + \beta_1\beta_0\gamma_0(\beta_1+8\gamma_1) - 4\beta_1^2\gamma_0^2)w^{1-\frac{4\gamma_0}{\beta_0}}}{\beta_0^4(\beta_0-4\gamma_0)} \\ &+ \frac{-\frac{\gamma_1(\beta_1-4\gamma_1)}{\gamma_0} + \beta_2 - 4\gamma_2}{2(\beta_0^2-16\gamma_0^2)} + w^{-\frac{4\gamma_0}{\beta_0}-1}\{hl0_0\left(-\frac{4\beta_1\gamma_0}{\beta_0^2} + \frac{4\gamma_1}{\beta_0} - \frac{4\beta_1\gamma_0\log(w)}{\beta_0^2}\right) + hl0_1 + \frac{\beta_1^2\gamma_0\log^2(w)}{\beta_0^4} \\ &+ \left(\frac{2\beta_1^2\gamma_0}{\beta_0^4} - \frac{2\beta_1\gamma_1}{\beta_0^3} - \frac{2\beta_1}{3\beta_0^2}\right)\log(w) + \frac{1}{6\beta_0^4(\beta_0+4\gamma_0)}\{2\beta_0^2(3(\beta_2\gamma_0+4\gamma_1^2) - \beta_1(8\gamma_0+9\gamma_1)) \\ &+ \beta_0^3(-4\beta_1+16\gamma_1+6\gamma_2) + 6\beta_1\beta_0\gamma_0(\beta_1-8\gamma_1) + 24\beta_1^2\gamma_0^2 - 3\beta_0^4\gamma_2^{ii}\}\}, \end{aligned} \tag{C9}$$

$$\begin{aligned} k_0^L(w) = &-\frac{w^{1-\frac{4\gamma_0}{\beta_0}}-1}{3(\beta_0-4\gamma_0)x} - \frac{1}{9\gamma_0} + \frac{\beta_1-4\gamma_1}{12\gamma_0(\beta_0-4\gamma_0)} + \frac{4(\beta_0\gamma_1-\beta_1\gamma_0)w^{1-\frac{4\gamma_0}{\beta_0}}}{3\beta_0^2(\beta_0-4\gamma_0)} \\ &+ w^{-\frac{4\gamma_0}{\beta_0}}\left(kl0_0 + \frac{-3\beta_0(\beta_1-4\gamma_1) + 4\beta_0^2 - 12\beta_1\gamma_0(\log(w)+1)}{36\beta_0^2\gamma_0}\right), \end{aligned} \tag{C10}$$

$$\begin{aligned} k_1^L(w) = &\, kl0_1 w^{-\frac{4\gamma_0}{\beta_0}-1} + \frac{2\beta_1\log(w)w^{-\frac{4\gamma_0}{\beta_0}-1}(2\beta_0\gamma_1 w + \beta_1\gamma_0(\log(w)-2w))}{3\beta_0^4} + \frac{\gamma_1(4\gamma_1-\beta_1)+\gamma_0(\beta_2-4\gamma_2)}{3\gamma_0(\beta_0^2-16\gamma_0^2)} \\ &+ \frac{3\gamma_0\gamma_2^{ii}+4\gamma_1}{9\gamma_0(\beta_0+4\gamma_0)} - \frac{4\beta_1\log(w)(3\beta_0\gamma_1 - 3\beta_1\gamma_0 + \beta_0^2(9\gamma_0 kl0_0+1))w^{-\frac{4\gamma_0}{\beta_0}-1}}{9\beta_0^4} + \frac{w^{-\frac{4\gamma_0}{\beta_0}-1}}{9\beta_0^4(\beta_0+4\gamma_0)}\{6\beta_1\beta_0\gamma_0 \\ &\times(\beta_1-8\gamma_1) - 2\beta_0^2(\beta_1(9\gamma_1+8\gamma_0(9\gamma_0 kl0_0+1)) - 3(\beta_2\gamma_0+4\gamma_1^2)) + \beta_0^4(36\gamma_1 kl0_0 - 3\gamma_2^{ii}) + 24\beta_1^2\gamma_0^2 \\ &+ 2\beta_0^3(3\gamma_2 - 2(\beta_1-4\gamma_1)(9\gamma_0 kl0_0+1))\} - \frac{4w^{-\frac{4\gamma_0}{\beta_0}-1}}{9\beta_0^4}\beta_1\log(w)(3\beta_0\gamma_1 - 3\beta_1\gamma_0 + \beta_0^2(9\gamma_0 kl0_0+1)) \\ &+ \frac{2w^{1-\frac{4\gamma_0}{\beta_0}}}{3\beta_0^4(\beta_0-4\gamma_0)}(\beta_0^3\gamma_2 - \beta_0^2(\beta_2\gamma_0+\gamma_1(\beta_1+4\gamma_1)) + \beta_1\beta_0\gamma_0(\beta_1+8\gamma_1) - 4\beta_1^2\gamma_0^2) + \frac{w^{-\frac{4\gamma_0}{\beta_0}}}{9\beta_0^4\gamma_0}\{24\beta_1\beta_0\gamma_0\gamma_1 \\ &- 12\beta_1^2\gamma_0^2 - 4\beta_0^3\gamma_1(9\gamma_0 kl0_0+1) + \beta_0^2(\beta_1(3\gamma_1+4\gamma_0(9\gamma_0 kl0_0+1)) - 3(\beta_2\gamma_0+4\gamma_1^2))\}, \end{aligned} \tag{C11}$$

where $w = (1-\beta_0 xL)$.

APPENDIX D: CONTRIBUTIONS TO THE ADLER FUNCTION

1. Dimension-zero contributions

In the massless case, the Adler function is known to $\mathcal{O}(\alpha_s^4)$ [41–50], and the contribution from the longitudinal part is zero ($D_{i,j}^{L,(0)} = 0$) while $D_{i,j}^{L+T,0}$ is given by

$$\mathcal{D}_{i,j}^{L+T,0} = 1 + x + x^2\left(\frac{299}{24} - 9\zeta(3)\right) + x^3\left(-\frac{779\zeta(3)}{4} + \frac{75\zeta(5)}{2} + \frac{58057}{288}\right) + x^4\left(\frac{4185\zeta(3)^2}{8} + \frac{729\pi^2\zeta(3)}{16} - \frac{1704247\zeta(3)}{432} + \frac{34165\zeta(5)}{96} - \frac{1995\zeta(7)}{16} - \frac{13365\pi^2}{256} + \frac{78631453}{20736}\right). \tag{D1}$$

2. Dimension-2 corrections

The dimension-2 correction to the Adler function for the quark flavors i and j is known to $\mathcal{O}(\alpha_s^3)$ [51–56], and the analytic expression reads

$$\begin{aligned}\mathcal{D}_{2,ij}^{L+T,V/A}(s) = \frac{3}{4\pi^2 s}\Bigg\{&(m_u^2 + m_d^2 + m_s^2)\left(x^2\left(\frac{8\zeta(3)}{3} - \frac{32}{9}\right) + x^3\left(4\zeta(3)^2 + \frac{1592\zeta(3)}{27} - \frac{80\zeta(5)}{27} - \frac{2222}{27}\right)\right)\\ &+ (m_i^2 + m_j^2)\left(1 + \frac{13x}{3} + x^2\left(\frac{179\zeta(3)}{54} - \frac{520\zeta(5)}{27} + \frac{23077}{432}\right)\right.\\ &\left.+ x^3\left(\frac{53\zeta(3)^2}{2} - \frac{1541\zeta(3)}{648} + \frac{79835\zeta(7)}{648} - \frac{54265\zeta(5)}{108} - \frac{\pi^4}{36} + \frac{3909929}{5184}\right)\right)\\ &\pm m_i m_j\left(\frac{2x}{3} + x^2\left(-\frac{55\zeta(3)}{27} - \frac{5\zeta(5)}{27} + \frac{769}{54}\right)\right.\\ &\left.+ x^3\left(-\frac{11677\zeta(3)^2}{108} + \frac{70427\zeta(3)}{324} + \frac{82765\zeta(5)}{54} - \frac{555233\zeta(7)}{864} + \frac{\pi^4}{9} - \frac{7429573}{3888}\right)\right)\Bigg\},\end{aligned} \tag{D2}$$

where upper and lower signs correspond to vector and axial-vector components, respectively, and this convention is used for the Alder functions in this appendix. It should be noted that the $\mathcal{O}(\alpha_s^4)$ correction to the $m_i m_j$ term has been obtained from Eq. (15) of Ref. [51]. The longitudinal component of the dimension-2 operator is known to $\mathcal{O}(\alpha_s^4)$ [9–14] and has the form

$$\mathcal{D}_{2,ij}^{L,V/A} = \frac{-3}{8\pi^2}\frac{(m_i \mp m_j)^2}{M_\tau^2}\left\{1 + \frac{17x}{3} + x^2\left(\frac{9631}{144} - \frac{35\zeta(3)}{2}\right) + x^3\left(-\frac{91519\zeta(3)}{216} + \frac{715\zeta(5)}{12} - \frac{\pi^4}{36} + \frac{4748953}{5184}\right) + x^4\left(\frac{192155\zeta(3)^2}{216} - \frac{46217501\zeta(3)}{5184} + \frac{455725\zeta(5)}{432} - \frac{125\pi^6}{9072} - \frac{52255\zeta(7)}{256} - \frac{3491\pi^4}{10368} + \frac{7055935615}{497664}\right)\right\}. \tag{D3}$$

From the above dimension-2 Alder functions, the important pieces relevant for Cabibbo suppressed strange quark mass determination [22] using Eq. (13) are

$$\begin{aligned}\delta\mathcal{D}_2^{L+T,V+A}(s) &= (\mathcal{D}_{2,ud}^{L+T,V+A}(s) - \mathcal{D}_{2,us}^{L+T,V+A}(s))\\ &= \frac{-3m_s^2}{2\pi^2 s}(1 - \epsilon_d^2)\left(1 + \frac{13x}{3} + x^2\left(\frac{179\zeta(3)}{54} - \frac{520\zeta(5)}{27} + \frac{23077}{432}\right)\right.\\ &\left.+ x^3\left(\frac{53\zeta(3)^2}{2} - \frac{1541\zeta(3)}{648} + \frac{79835\zeta(7)}{648} - \frac{54265\zeta(5)}{108} - \frac{\pi^4}{36} + \frac{3909929}{5184}\right)\right)\end{aligned} \tag{D4}$$

$$\equiv \frac{-3m_s^2(-\xi^2 s)}{2\pi^2 s}(1 - \epsilon_d^2)\sum_{i=0}\tilde{d}_{i,0}^{L+T}(\xi^2)x(-\xi^2 s)^i \tag{D5}$$

$$= \frac{-3m_s^2(\xi^2 M_\tau^2)}{2\pi^2 s}(1 - \epsilon_d^2)\sum_{i=0}^{4}\sum_{j=0}^{i}\tilde{d}_{i,j}^{L+T}x(\xi^2 M_\tau^2)^i \log^j\left(\frac{\xi^2 M_\tau^2}{-s}\right), \tag{D6}$$

and the corresponding contribution from the longitudinal component is

$$\begin{aligned}\delta\mathcal{D}_2^{L,V+A}(s) &= \mathcal{D}_{2,ud}^{L,V+A} - \mathcal{D}_{2,us}^{L,V+A} \\ &= \frac{3m_s^2}{4\pi^2 M_\tau^2}(1-\epsilon_d^2)\left\{1+\frac{17x}{3}+x^2\left(\frac{9631}{144}-\frac{35\zeta(3)}{2}\right)+x^3\left(-\frac{91519\zeta(3)}{216}+\frac{715\zeta(5)}{12}-\frac{\pi^4}{36}+\frac{4748953}{5184}\right)\right. \\ &\quad \left.+x^4\left(\frac{192155\zeta(3)^2}{216}-\frac{46217501\zeta(3)}{5184}+\frac{455725\zeta(5)}{432}-\frac{52255\zeta(7)}{256}-\frac{125\pi^6}{9072}-\frac{3491\pi^4}{10368}+\frac{7055935615}{497664}\right)\right\} \quad \text{(D7)} \\ &\equiv \frac{3m_s^2(-\xi^2 s)}{4\pi^2 M_\tau^2}(1-\epsilon_d^2)\sum_{i=0}\tilde{d}_{i,0}^{L}(\xi^2)x(-\xi^2 s)^i \quad \text{(D8)} \\ &= \frac{3m_s^2(\xi^2 M_\tau^2)}{4\pi^2 M_\tau^2}(1-\epsilon_d^2)\sum_{i=0}^{4}\sum_{j=0}^{i}\tilde{d}_{i,j}^{L}x(\xi^2 M_\tau^2)^i\log^j\left(\frac{\xi^2 M_\tau^2}{-s}\right). \quad \text{(D9)}\end{aligned}$$

The RGSPT coefficients for the dimension-2 operators can be written in the following form:

$$\begin{aligned}\delta\mathcal{D}_{V+A}^{J,2}(s) &= \text{norm}\times\frac{3m_s^2}{2\pi^2}(1-\epsilon_d^2)\left\{\frac{1}{w^{8/9}}+x\left(\frac{\tilde{d}_{1,0}^J}{w^{17/9}}-\frac{1.79012}{w^{8/9}}+\frac{1.79012}{w^{17/9}}-\frac{1.58025\log(w)}{w^{17/9}}\right)\right. \\ &\quad +x^2\left(\frac{1.79012\tilde{d}_{1,0}^J}{w^{26/9}}+\frac{\tilde{d}_{2,0}^J}{w^{26/9}}-\frac{1.79012\tilde{d}_{1,0}^J}{w^{17/9}}+\frac{(-3.35802\tilde{d}_{1,0}^J-8.82061)\log(w)}{w^{26/9}}-\frac{0.339459}{w^{8/9}}\right. \\ &\quad \left.-\frac{4.36949}{w^{17/9}}+\frac{4.70895}{w^{26/9}}+\frac{2.65325\log^2(w)}{w^{26/9}}+\frac{2.82884\log(w)}{w^{17/9}}\right) \\ &\quad +x^3\left(\frac{6.01952\tilde{d}_{1,0}^J}{w^{35/9}}+\frac{1.79012\tilde{d}_{2,0}^J}{w^{35/9}}+\frac{\tilde{d}_{3,0}^J}{w^{35/9}}-\frac{0.339459\tilde{d}_{1,0}^J}{w^{17/9}}-\frac{5.68006\tilde{d}_{1,0}^J}{w^{26/9}}-\frac{1.79012\tilde{d}_{2,0}^J}{w^{26/9}}\right. \\ &\quad +\frac{(8.62308\tilde{d}_{1,0}^J+27.3673)\log^2(w)}{w^{35/9}}+\frac{(6.01128\tilde{d}_{1,0}^J+19.7019)\log(w)}{w^{26/9}}+\frac{0.593473}{w^{8/9}} \\ &\quad -\frac{3.28306}{w^{17/9}}+\frac{(-15.1635\tilde{d}_{1,0}^J-5.1358\tilde{d}_{2,0}^J-39.8653)\log(w)}{w^{35/9}}-\frac{14.9321}{w^{26/9}}+\frac{17.6217}{w^{35/9}} \\ &\quad \left.-\frac{4.5422\log^3(w)}{w^{35/9}}-\frac{4.74965\log^2(w)}{w^{26/9}}+\frac{0.53643\log(w)}{w^{17/9}}\right) \\ &\quad +x^4\left(\frac{0.593473\tilde{d}_{1,0}^J}{w^{17/9}}+\frac{27.6536\tilde{d}_{1,0}^J}{w^{44/9}}+\frac{7.3301\tilde{d}_{2,0}^J}{w^{44/9}}+\frac{1.79012\tilde{d}_{3,0}^J}{w^{44/9}}+\frac{\tilde{d}_{4,0}^J}{w^{44/9}}-\frac{6.29286\tilde{d}_{1,0}^J}{w^{26/9}}\right. \\ &\quad -\frac{0.339459\tilde{d}_{2,0}^J}{w^{26/9}}-\frac{21.9542\tilde{d}_{1,0}^J}{w^{35/9}}-\frac{6.99064\tilde{d}_{2,0}^J}{w^{35/9}}-\frac{1.79012\tilde{d}_{3,0}^J}{w^{35/9}}-\frac{12.673}{w^{8/9}}+\frac{11.6487}{w^{17/9}} \\ &\quad +\frac{(1.13991\tilde{d}_{1,0}^J+11.9782)\log(w)}{w^{26/9}}+\frac{(-19.8721\tilde{d}_{1,0}^J-71.1438)\log^3(w)}{w^{44/9}}-\frac{15.09}{w^{26/9}} \\ &\quad +\frac{(-15.4364\tilde{d}_{1,0}^J-59.0364)\log^2(w)}{w^{35/9}}-\frac{60.9336}{w^{35/9}}+\frac{77.0479}{w^{44/9}}+\frac{8.13109\log^3(w)}{w^{35/9}} \\ &\quad -\frac{(68.5739\tilde{d}_{1,0}^J+21.5065\tilde{d}_{2,0}^J+6.91358\tilde{d}_{3,0}^J+192.701)\log(w)}{w^{44/9}}-\frac{0.937834\log(w)}{w^{17/9}} \\ &\quad +\frac{(39.8584\tilde{d}_{1,0}^J+9.19372\tilde{d}_{2,0}^J+111.714)\log(w)}{w^{35/9}}+\frac{7.85071\log^4(w)}{w^{44/9}}-\frac{0.900672\log^2(w)}{w^{26/9}} \\ &\quad \left.\left.+\frac{(67.7471\tilde{d}_{1,0}^J+17.7534\tilde{d}_{2,0}^J+186.459)\log^2(w)}{w^{44/9}}\right)\right\}. \quad \text{(D10)}\end{aligned}$$

A more compact form for the above equation is

$$\delta\mathcal{D}^{J,2}_{V+A}(s) \equiv \text{norm} \times \frac{3m_s^2}{2\pi^2}(1-\epsilon_d^2)\sum_{i=0}^{4}\sum_{k=0}^{i}\sum_{j=0}^{k} x^i \tilde{T}^J_{i,j,k}\frac{\log^j(w)}{w^{2\gamma_0/\beta_0+k}}, \tag{D11}$$

where

$$\text{norm} = \begin{cases} \frac{-1}{s} & \text{if } J=0+1 \\ \frac{1}{2M_\tau^2} & J=0, \end{cases} \tag{D12}$$

and $\tilde{d}_i^J$ can be obtained from Eqs. (D5) and (D8).

APPENDIX E: DETAILS OF m_s AND $|V_{us}|$ DETERMINATIONS IN DIFFERENT SCHEMES AND THE DETAILS OF SOURCES OF UNCERTAINTY

1. Strange quark mass determinations using pQCD inputs

In this section, the strange quark mass is calculated using the longitudinal component with the OPE as described in Sec. V. As mentioned before, these contributions are poorly convergent, and the strange quark mass determinations will suffer from the large truncation uncertainties, in addition to significant dependence on the moments used. The dependence on the moment can be slightly reduced by using prescription I at the cost of enhanced truncation uncertainty. This behavior in the different perturbative schemes and the details of various sources of uncertainties are discussed in the later subsections.

a. Strange quark mass determination using CIPT scheme

Determination of $m_s(M_\tau^2)$ using CIPT is based on dimension-2 contributions described in Sec. V A. Using prescription I, we can see that dimension-2 contributions are truncated at $\mathcal{O}(\alpha_s^3)$, $\mathcal{O}(\alpha_s^3)$, $\mathcal{O}(\alpha_s^2)$, and $\mathcal{O}(\alpha_s)$ for $k=0$, 1, 2, 3, and 4, respectively. This truncation results in the enhancement in the total uncertainty in the $m_s(M_\tau^2)$ determination and can be seen in Tables X and XI. However, the main advantage of using prescription I is that the masses from various moments, using different experimental inputs, agree within the uncertainty, which is not the case in using prescription 2. For this reason, we present $m_s(M_\tau^2)$ from both prescriptions for different schemes in other cases, too.

b. Strange quark mass determination using FOPT scheme

The effect of different prescriptions used is very significant in the FOPT where perturbative contributions from dimension-2 Alder functions are truncated at $\mathcal{O}(\alpha_s^4)$ and $\mathcal{O}(\alpha_s^2)$ for the moment $k=0$ and 1 while the rest of them are truncated at $\mathcal{O}(\alpha_s)$. The final results for $m_s(M_\tau^2)$ determination using FOPT in prescriptions I and II are presented in Tables XII and XIII, respectively.

TABLE X. Strange quark mass using CIPT in prescription I. Other sources of uncertainties are not shown in the table, but they are added in quadrature for $m_s(M_\tau^2)$ in the second row.

	Moments ALEPH [32]					Moment OPAL [27]				
Parameter	(0, 0)	(1, 0)	(2, 0)	(3, 0)	(4, 0)	(0, 0)	(1, 0)	(2, 0)	(3, 0)	(4, 0)
$m_s(M_\tau^2)$	135^{+34}_{-37}	122^{+28}_{-24}	120^{+32}_{-24}	105^{+31}_{-23}	108^{+38}_{-24}	124^{+30}_{-31}	106^{+27}_{-26}	105^{+30}_{-25}	94^{+29}_{-22}	100^{+36}_{-24}
δR_τ^{kl}(Exp.)	$^{+27.4}_{-34.8}$	$^{+15.4}_{-17.7}$	$^{+11.7}_{-13.0}$	$^{+9.4}_{-10.4}$	$^{+9.0}_{-9.9}$	$^{+23.2}_{-28.7}$	$^{+17.8}_{-21.6}$	$^{+14.4}_{-16.8}$	$^{+11.2}_{-12.8}$	$^{+10.6}_{-12.0}$
$\xi \in [0.75, 2.0]$	$^{+14.3}_{-6.2}$	$^{+17.3}_{-8.0}$	$^{+20.8}_{-10.4}$	$^{+21.1}_{-10.9}$	$^{+23.8}_{-13.4}$	$^{+13.4}_{-5.8}$	$^{+15.1}_{-7.1}$	$^{+18.5}_{-9.2}$	$^{+19.0}_{-9.9}$	$^{+22.1}_{-12.5}$
Truncation uncertainty	$^{-8.7}_{+10.7}$	$^{-9.4}_{+12.2}$	$^{-12.1}_{+17.3}$	$^{-11.4}_{+16.8}$	$^{-15.6}_{+26.7}$	$^{-8.0}_{+10.0}$	$^{-8.2}_{+10.6}$	$^{-10.7}_{+15.3}$	$^{-10.3}_{+15.2}$	$^{-14.5}_{+25.1}$
$s_0 \in [3, M_\tau^2](\text{GeV}^2)$	8.3	11.1	12.7	12.5	6.4	7.7	9.6	11.2	11.2	5.9

TABLE XI. CIPT determination of strange quark mass using prescription II. Only significant sources of uncertainty are shown separately, while the rest are added in quadrature and appear in $m_s(M_\tau^2)$.

	Moments ALEPH [32]					Moment OPAL [27]				
Parameter	(0, 0)	(1, 0)	(2, 0)	(3, 0)	(4, 0)	(0, 0)	(1, 0)	(2, 0)	(3, 0)	(4, 0)
$m_s(M_\tau^2)$	126^{+31}_{-35}	112^{+26}_{-22}	96^{+25}_{-19}	82^{+25}_{-18}	69^{+24}_{-17}	116^{+27}_{-29}	97^{+25}_{-24}	84^{+24}_{-20}	73^{+23}_{-18}	64^{+23}_{-16}
δR_τ^{kl}(Exp.)	$^{+25.7}_{-32.6}$	$^{+14.1}_{-16.3}$	$^{+9.5}_{-10.5}$	$^{+7.4}_{-8.1}$	$^{+5.9}_{-6.4}$	$^{+21.7}_{-26.9}$	$^{+16.4}_{-19.8}$	$^{+11.6}_{-13.6}$	$^{+8.8}_{-10.0}$	$^{+6.9}_{-7.8}$
$\xi \in [0.75, 2.0]$	$^{+13.2}_{-6.4}$	$^{+16.3}_{-8.3}$	$^{+18.0}_{-9.4}$	$^{+18.7}_{-10.0}$	$^{+18.6}_{-10.1}$	$^{+12.3}_{-6.0}$	$^{+14.3}_{-7.2}$	$^{+15.9}_{-8.3}$	$^{+16.8}_{-9.0}$	$^{+17.1}_{-9.3}$
Truncation uncertainty	$^{-7.3}_{+8.8}$	$^{-8.0}_{+10.1}$	$^{-8.0}_{+10.6}$	$^{-7.7}_{+10.6}$	$^{-7.2}_{+10.4}$	$^{-6.7}_{+8.1}$	$^{-6.9}_{+8.8}$	$^{-7.0}_{+9.3}$	$^{-6.9}_{+9.6}$	$^{-6.6}_{+9.6}$
$s_0 \in [3, M_\tau^2](\text{GeV}^2)$	7.8	10.2	10.2	9.7	9.1	7.2	8.8	9.0	8.7	8.5

TABLE XII. Strange quark mass using FOPT in prescription I. Other sources of uncertainties are not shown in the table but are added in quadrature and appear for $m_s(M_\tau^2)$ in the second row.

	Moments ALEPH [32]					Moment OPAL [27]				
Parameter	(0, 0)	(1, 0)	(2, 0)	(3, 0)	(4, 0)	(0, 0)	(1, 0)	(2, 0)	(3, 0)	(4, 0)
$m_s(M_\tau^2)$	114^{+33}_{-34}	134^{+38}_{-30}	147^{+48}_{-34}	137^{+45}_{-31}	127^{+29}_{-29}	106^{+29}_{-29}	116^{+35}_{-31}	130^{+45}_{-33}	124^{+43}_{-30}	118^{+40}_{-29}
δR_τ^{kl}(Exp.)	$^{+23.2}_{-29.3}$	$^{+16.5}_{-19.0}$	$^{+13.7}_{-15.4}$	$^{+11.5}_{-12.8}$	$^{+9.9}_{-11.0}$	$^{+19.6}_{-24.2}$	$^{+19.1}_{-23.2}$	$^{+17.0}_{-19.9}$	$^{+13.9}_{-16.0}$	$^{+11.8}_{-13.5}$
$\xi \in [0.75, 2.0]$	$^{+19.0}_{-11.0}$	$^{+22.6}_{-12.8}$	$^{+23.7}_{-13.5}$	$^{+21.7}_{-12.3}$	$^{+19.5}_{-11.1}$	$^{+17.6}_{-10.2}$	$^{+19.8}_{-11.2}$	$^{+21.2}_{-12.0}$	$^{+19.7}_{-11.1}$	$^{+18.0}_{-10.2}$
Truncation uncertainty	$^{-8.0}_{+10.1}$	$^{-14.7}_{+21.7}$	$^{-21.5}_{+36.7}$	$^{-20.2}_{+34.5}$	$^{-18.9}_{+32.2}$	$^{-7.4}_{+9.3}$	$^{-12.8}_{+19.0}$	$^{-19.2}_{+33.3}$	$^{-18.5}_{+32.1}$	$^{-17.8}_{+30.7}$
$s_0 \in [3, M_\tau^2](\mathrm{GeV}^2)$	8.7	13.2	15.7	15.3	15.4	8.0	11.5	13.9	13.8	14.3

TABLE XIII. Strange quark mass using FOPT in prescription II. Other sources of uncertainties are not shown in the table but are added in quadrature and appear for $m_s(M_\tau^2)$ in the second row.

	Moments ALEPH [32]					Moment OPAL [27]				
Parameter	(0, 0)	(1, 0)	(2, 0)	(3, 0)	(4, 0)	(0, 0)	(1, 0)	(2, 0)	(3, 0)	(4, 0)
$m_s(M_\tau^2)$	114^{+33}_{-34}	107^{+30}_{-24}	97^{+28}_{-20}	87^{+27}_{-20}	78^{+25}_{-19}	106^{+29}_{-29}	93^{+28}_{-25}	85^{+26}_{-21}	78^{+25}_{-19}	72^{+24}_{-18}
δR_τ^{kl}(Exp.)	$^{+23.2}_{-29.3}$	$^{+13.3}_{-15.2}$	$^{+9.3}_{-10.4}$	$^{+7.6}_{-8.4}$	$^{+6.5}_{-7.1}$	$^{+19.6}_{-24.2}$	$^{+15.3}_{-18.5}$	$^{+11.4}_{-13.3}$	$^{+9.1}_{-10.4}$	$^{+7.6}_{-8.6}$
$\xi \in [0.75, 2.0]$	$^{+19.0}_{-11.0}$	$^{+20.8}_{-12.2}$	$^{+20.8}_{-12.2}$	$^{+19.8}_{-11.7}$	$^{+18.4}_{-10.8}$	$^{+17.6}_{-10.2}$	$^{+18.1}_{-10.6}$	$^{+18.2}_{-10.7}$	$^{+17.7}_{-10.4}$	$^{+16.9}_{-9.9}$
Truncation uncertainty	$^{-8.0}_{+10.1}$	$^{-9.0}_{+12.0}$	$^{-9.1}_{+12.7}$	$^{-8.9}_{+12.8}$	$^{-8.5}_{+12.5}$	$^{-7.4}_{+9.3}$	$^{-7.8}_{+10.5}$	$^{-8.1}_{+11.2}$	$^{-8.0}_{+11.5}$	$^{-7.8}_{+11.6}$
$s_0 \in [3, M_\tau^2](\mathrm{GeV}^2)$	8.7	10.5	10.6	10.3	10.1	8.0	9.1	9.3	9.3	9.4

c. Strange quark mass determination using the RGSPT scheme

The RGSPT determination of strange quark mass is presented in Tables XIV and XV, and the most crucial feature of this scheme is that it provides minimum scale uncertainty compared to the CIPT and FOPT. Another important advantage we can infer from prescription II is that it gives the lowest uncertainty among other perturbative schemes.

TABLE XIV. Strange quark mass using RGSPT in prescription I. Other sources of uncertainties are not shown in the table but are added in quadrature and appear for $m_s(M_\tau^2)$ in the second row.

	Moments ALEPH [32]					Moment OPAL [27]				
Parameter	(0, 0)	(1, 0)	(2, 0)	(3, 0)	(4, 0)	(0, 0)	(1, 0)	(2, 0)	(3, 0)	(4, 0)
$m_s(M_\tau^2)$	123^{+28}_{-34}	121^{+23}_{-23}	120^{+26}_{-23}	125^{+37}_{-27}	113^{+35}_{-25}	114^{+24}_{-28}	104^{+23}_{-25}	105^{+25}_{-24}	113^{+35}_{-27}	104^{+33}_{-25}
δR_τ^{kl} (Exp.)	$^{+25.2}_{-32.0}$	$^{+15.2}_{-17.4}$	$^{+11.6}_{-13.0}$	$^{+10.9}_{-12.0}$	$^{+9.1}_{-10.1}$	$^{+21.3}_{-26.3}$	$^{+17.5}_{-21.2}$	$^{+14.3}_{-16.7}$	$^{+13.1}_{-15.0}$	$^{+10.8}_{-12.3}$
$\xi \in [0.75, 2]$	$^{+3.3}_{-2.1}$	$^{+4.3}_{-2.8}$	$^{+5.1}_{-3.4}$	$^{+6.2}_{-4.2}$	$^{+5.9}_{-4.0}$	$^{+3.0}_{-2.0}$	$^{+3.7}_{-2.4}$	$^{+4.6}_{-3.0}$	$^{+5.7}_{-3.8}$	$^{+5.5}_{-3.7}$
Truncation uncertainty	$^{-7.2}_{+8.7}$	$^{-9.7}_{+12.8}$	$^{-12.7}_{+18.5}$	$^{-18.2}_{+31.3}$	$^{-16.9}_{+29.6}$	$^{-6.7}_{+8.1}$	$^{-8.4}_{+11.1}$	$^{-11.2}_{+16.4}$	$^{-16.5}_{+28.8}$	$^{-15.8}_{+27.9}$
$s_0 \in [3, M_\tau^2](\mathrm{GeV}^2)$	8.1	11.4	13.1	15.1	14.6	7.5	9.9	11.5	13.6	13.5

TABLE XV. RGSPT determination of strange quark mass using prescription II. Only the main sources of uncertainty are shown separately, while the rest are added directly in quadrature of $m_s(M_\tau^2)$.

	Moments ALEPH [32]					Moment OPAL [27]				
Parameter	(0, 0)	(1, 0)	(2, 0)	(3, 0)	(4, 0)	(0, 0)	(1, 0)	(2, 0)	(3, 0)	(4, 0)
$m_s(M_\tau^2)$	123^{+28}_{-34}	110^{+21}_{-21}	95^{+18}_{-17}	82^{+17}_{-16}	70^{+16}_{-14}	114^{+24}_{-28}	95^{+21}_{-23}	84^{+18}_{-18}	74^{+17}_{-16}	65^{+16}_{-14}
δR_τ^{kl}(Exp.)	$^{+25.2}_{-32.0}$	$^{+13.9}_{-16.0}$	$^{+9.4}_{-10.4}$	$^{+7.3}_{-8.1}$	$^{+5.9}_{-6.5}$	$^{+21.3}_{-26.3}$	$^{+16.1}_{-19.4}$	$^{+11.5}_{-13.4}$	$^{+8.8}_{-10.0}$	$^{+7.0}_{-7.9}$
$\xi \in [0.75, 2.0]$	$^{+3.3}_{-2.1}$	$^{+4.0}_{-2.6}$	$^{+4.3}_{-2.8}$	$^{+4.4}_{-2.9}$	$^{+4.4}_{-2.9}$	$^{+3.0}_{-2.0}$	$^{+3.4}_{-2.3}$	$^{+3.8}_{-2.5}$	$^{+4.0}_{-2.6}$	$^{+4.1}_{-2.7}$
Truncation uncertainty	$^{-7.2}_{+8.7}$	$^{-8.1}_{+10.3}$	$^{-8.2}_{+10.9}$	$^{-7.9}_{+11.1}$	$^{-7.5}_{+10.9}$	$^{-6.7}_{+8.1}$	$^{-7.0}_{+8.9}$	$^{-7.2}_{+9.6}$	$^{-7.1}_{+10.0}$	$^{-6.9}_{+10.1}$
$s_0 \in [3, M_\tau^2](\mathrm{GeV}^2)$	8.1	10.4	10.4	9.9	9.3	7.5	9.0	9.1	8.9	8.6

2. Strange quark mass determinations using phenomenological inputs

In this section, the strange quark mass is calculated using the phenomenological parametrization along with the perturbative $L+T$ contributions described in Secs. VI and IV. The quark mass is calculated in the two prescriptions for various moments, and the details of sources of uncertainty are presented in the tables.

a. Strange quark mass determination using CIPT scheme

The CIPT determination of $m_s(M_\tau^2)$ in this section makes use of the full dimension-2 results of $\mathcal{O}(\alpha_s^3)$ as the series presented in Eq. (41) is convergent for all moments, and prescriptions I and II yield the same determinations. The results are shown in Table XVI.

b. Strange quark mass determination using the FOPT scheme

The FOPT determination of $m_s(M_\tau^2)$ in this section involves determination in both prescriptions I and II as the perturbation series is not well convergent for different moments, as shown in Eq. (47). The results are presented in Tables XVII and XVIII.

c. Strange quark mass determination using the RGSPT scheme

The RGSPT determination in prescriptions I and II is shown in Table XIX as the (4, 0) moment is not convergent term by term until $\mathcal{O}(\alpha_s^3)$.

TABLE XVI. Strange quark mass using CIPT with phenomenological inputs for the longitudinal component. Only the main sources of uncertainty are shown separately, while the rest are already added in quadrature and appear in the total uncertainty in $m_s(M_\tau^2)$.

	Moments ALEPH [32]						Moment OPAL [27]					
Parameter	(0, 0)	(1, 0)	(2, 0)	(3, 0)	(4, 0)	(4,0)[a]	(0, 0)	(1, 1)	(2, 0)	(3, 0)	(4, 0)	(4,0)[a]
$m_s(M_\tau^2)$	187^{+63}_{-81}	162^{+31}_{-34}	136^{+25}_{-24}	115^{+25}_{-20}	98^{+22}_{-15}	98^{+25}_{-19}	166^{+54}_{-69}	134^{+34}_{-41}	116^{+26}_{-27}	102^{+24}_{-21}	91^{+21}_{-16}	91^{+24}_{-19}
δR_τ^{kl}(Exp.)	$^{+57.2}_{-79.0}$	$^{+25.5}_{-30.1}$	$^{+15.5}_{-17.5}$	$^{+11.4}_{-12.7}$	$^{+8.8}_{-9.7}$	$^{+8.8}_{-9.7}$	$^{+49.0}_{-67.8}$	$^{+30.2}_{-39.0}$	$^{+19.4}_{-23.3}$	$^{+13.8}_{-16.0}$	$^{+10.5}_{-11.9}$	$^{+10.5}_{-11.9}$
$\xi \in [0.75, 2.0]$	$^{-9.5}_{+22.9}$	$^{-1.0}_{+9.1}$	$^{+10.8}_{-0.1}$	$^{+14.4}_{-1.7}$	$^{+16.3}_{-3.8}$	$^{+16.3}_{-3.8}$	$^{-7.9}_{+19.5}$	$^{-0.7}_{+7.1}$	$^{+9.5}_{-0.2}$	$^{+12.8}_{-1.6}$	$^{+14.8}_{-3.5}$	$^{+14.8}_{-3.5}$
Truncation uncertainty	$^{+3.3}_{-3.1}$	$^{-4.5}_{+4.9}$	$^{-7.1}_{+8.4}$	$^{-7.9}_{+10.0}$	$^{-8.1}_{+10.8}$	$^{+2.8}_{-2.7}$	$^{+2.8}_{-2.7}$	$^{-3.7}_{+4.0}$	$^{-6.0}_{+7.1}$	$^{-7.0}_{+8.9}$	$^{-7.5}_{+9.9}$	$^{-7.5}_{+9.9}$
$s_0 \in [3, M_\tau^2](\mathrm{GeV}^2)$	11.6	14.7	14.5	13.7	5.8	13.0	10.2	12.9	12.8	12.2	5.2	11.7

[a]Prescription II is used for these moments.

TABLE XVII. FOPT determination of $m_s(M_\tau^2)$ using prescription I. Only major sources of uncertainty are shown separately, while the rest are added in quadrature and appear in the total uncertainty in $m_s(M_\tau^2)$.

	Moments ALEPH [32]					Moment OPAL [27]				
Parameter	(0, 0)	(1, 0)	(2, 0)	(3, 0)	(4, 0)	(0, 0)	(1, 0)	(2, 0)	(3, 0)	(4, 0)
$m_s(M_\tau^2)$	141^{+46}_{-60}	133^{+35}_{-31}	135^{+38}_{-29}	145^{+50}_{-33}	135^{+46}_{-31}	125^{+40}_{-51}	111^{+34}_{-35}	116^{+36}_{-30}	130^{+46}_{-33}	125^{+44}_{-30}
$\delta R_\tau^{kl}(M_\tau^2)$(Exp.)	$^{+41.2}_{-57.9}$	$^{+20.5}_{-24.2}$	$^{+15.0}_{-16.9}$	$^{+13.8}_{-15.4}$	$^{+11.4}_{-12.7}$	$^{+35.6}_{-49.8}$	$^{+24.3}_{-31.2}$	$^{+18.7}_{-22.5}$	$^{+16.7}_{-19.5}$	$^{+13.6}_{-15.6}$
$\xi \in [0.75, 2]$	$^{+16.5}_{-6.4}$	$^{+21.7}_{-10.5}$	$^{+24.5}_{-12.0}$	$^{+25.5}_{-12.6}$	$^{+23.0}_{-11.4}$	$^{+14.8}_{-5.8}$	$^{+18.1}_{-8.8}$	$^{+21.0}_{-10.3}$	$^{+22.7}_{-11.2}$	$^{+21.1}_{-10.4}$
Truncation uncertainty	$^{-5.8}_{+6.7}$	$^{-9.7}_{+12.4}$	$^{-14.4}_{+21.1}$	$^{-21.2}_{+36.8}$	$^{-19.9}_{+34.4}$	$^{-5.1}_{+5.9}$	$^{-8.0}_{+10.2}$	$^{-12.4}_{+18.2}$	$^{-19.0}_{+33.4}$	$^{-18.6}_{+32.4}$
$s_0 \in [3, M_\tau^2](\mathrm{GeV}^2)$	10.7	13.1	14.4	16.2	16.3	9.5	11.6	12.8	14.6	14.9

TABLE XVIII. FOPT determination of $m_s(M_\tau^2)$ in prescription II. Only major sources of uncertainty are shown separately, while the rest are added in quadrature and appear in the total uncertainty in $m_s(M_\tau^2)$.

	Moments ALEPH [32]					Moment OPAL [27]				
Parameter	(0, 0)	(1, 0)	(2, 0)	(3, 0)	(4, 0)	(0, 0)	(1, 0)	(2, 0)	(3, 0)	(4, 0)
$m_s(M_\tau^2)$	141^{+46}_{-60}	133^{+35}_{-31}	121^{+26}_{-33}	109^{+32}_{-23}	99^{+30}_{-22}	125^{+40}_{-51}	111^{+34}_{-35}	104^{+31}_{-27}	97^{+29}_{-23}	91^{+28}_{-22}
$\delta R_\tau^{kl}(M_\tau^2)$(Exp.)	$^{+41.2}_{-57.9}$	$^{+20.5}_{-24.2}$	$^{+15.0}_{-16.9}$	$^{+13.8}_{-15.4}$	$^{+11.4}_{-12.7}$	$^{+35.6}_{-49.8}$	$^{+24.3}_{-31.2}$	$^{+18.7}_{-22.5}$	$^{+16.7}_{-19.5}$	$^{+13.6}_{-15.6}$
$\xi \in [0.75, 2]$	$8^{+16.5}_{-6.4}$	$^{+21.7}_{-10.5}$	$^{+24.5}_{-12.0}$	$^{+25.5}_{-12.6}$	$^{+23.0}_{-11.4}$	$^{+14.8}_{-5.8}$	$^{+18.1}_{-8.8}$	$^{+21.0}_{-10.3}$	$^{+22.7}_{-11.2}$	$^{+21.1}_{-10.4}$
Truncation uncertainty	$^{-5.8}_{+6.7}$	$^{-9.7}_{+12.4}$	$^{-10.4}_{+14.5}$	$^{-10.7}_{+15.1}$	$^{-10.4}_{+15.2}$	$^{-5.1}_{+5.9}$	$^{-8.0}_{+10.2}$	$^{-9.2}_{+12.5}$	$^{-9.6}_{+13.5}$	$^{-9.7}_{+14.1}$
$s_0 \in [3, M_\tau^2](\mathrm{GeV}^2)$	10.7	13.1	13.3	13.0	12.8	9.5	11.6	11.7	11.6	11.7

TABLE XIX. Strange quark mass using RGSPT. Other sources of uncertainty are not shown in the table but are added in quadrature and appear for $m_s(M_\tau^2)$ in the second row.

	Moments ALEPH [32]						Moment OPAL [27]					
Parameter	(0, 0)	(1, 0)	(2, 0)	(3, 0)	(4, 0)	(4, 0)[a]	(0, 0)	(1, 0)	(2, 0)	(3, 0)	(4, 0)	(4, 0)[a]
$m_s(M_\tau^2)$(in MeV)	178^{+57}_{-77}	154^{+29}_{-33}	130^{+23}_{-23}	111^{+21}_{-20}	108^{+25}_{-21}	96^{+20}_{-18}	157^{+49}_{-66}	127^{+32}_{-39}	112^{+24}_{-26}	99^{+21}_{-21}	100^{+24}_{-21}	89^{+19}_{-18}
δR_τ^{kl}(Exp.)	$^{+55.8}_{-75.5}$	$^{+24.5}_{-28.7}$	$^{+14.9}_{-16.8}$	$^{+11.0}_{-12.2}$	$^{+9.6}_{-10.6}$	$^{+8.6}_{-9.4}$	$^{+47.4}_{-64.6}$	$^{+28.8}_{-37.0}$	$^{+18.5}_{-22.3}$	$^{+13.3}_{-15.4}$	$^{+11.4}_{-12.9}$	$^{+10.1}_{-11.5}$
$\xi \in [0.75, 2]$	$^{-2.7}_{+2.6}$	$^{+1.1}_{-0.2}$	$^{+2.9}_{-1.5}$	$^{+3.7}_{-2.1}$	$^{+4.6}_{-2.7}$	$^{+4.0}_{-2.3}$	$^{-2.2}_{+2.1}$	$^{+1.1}_{-0.3}$	$^{+2.5}_{-1.4}$	$^{+3.3}_{-1.9}$	$^{+4.3}_{-2.5}$	$^{+3.7}_{-2.2}$
Truncation uncertainty	$^{+2.9}_{-2.7}$	$^{-5.4}_{+6.1}$	$^{-7.9}_{+9.7}$	$^{-8.7}_{+11.3}$	$^{-11.6}_{+16.9}$	$^{-8.8}_{+12.1}$	$^{+2.5}_{-2.4}$	$^{-4.4}_{+4.9}$	$^{-6.8}_{+8.3}$	$^{-7.7}_{+10.1}$	$^{-10.7}_{+15.6}$	$^{-8.1}_{+11.1}$
$s_0 \in [3, M_\tau^2]$(GeV^2)	11.7	14.5	14.2	13.4	12.8	10.3	12.8	12.5	12.5	12.0	12.8	11.6

[a]Prescription II is used for these moments.

3. Details of the $|V_{us}|$ determinations from OPAL data

The CKM matrix element $|V_{us}|$ is calculated using Eq. (62) from the available data on moments for strange and nonstrange components. Details of extraction from these moments and associated uncertainties from the input parameters are presented in this section. Purely pQCD inputs for the longitudinal component are used to extract $|V_{us}|$ in Tables XX and XXI. Large theoretical uncertainties in prescription II come from the truncation of the perturbative series. Determination of $|V_{us}|$ from the phenomenological inputs for the longitudinal contribution is presented in Tables XXII and XXIII for prescriptions I and II, respectively.

TABLE XX. Determination of $|V_{us}|$ in various schemes from the OPAL data using prescription I. The longitudinal component is calculated using the pQCD Adler function.

	$\lvert V_{us}\rvert_{\mathrm{CIPT}}$					$\lvert V_{us}\rvert_{\mathrm{FOPT}}$					$\lvert V_{us}\rvert_{\mathrm{RGSPT}}$				
Parameters	(0, 0)	(1, 0)	(2, 0)	(3, 0)	(4, 0)	(0, 0)	(1, 0)	(2, 0)	(3, 0)	(4, 0)	(0, 0)	(1, 0)	(2, 0)	(3, 0)	(4, 0)
$\lvert V_{us}\rvert$ (central)	0.2217	0.2224	0.2219	0.2241	0.2220	0.2227	0.2208	0.2183	0.2181	0.2182	0.2221	0.2229	0.2223	0.2204	0.2217
m_s	$^{+0.0014}_{-0.0012}$	$^{+0.0021}_{-0.0018}$	$^{+0.0025}_{-0.0022}$	$^{+0.0038}_{-0.0032}$	$^{+0.0037}_{-0.0031}$	$^{+0.0017}_{-0.0015}$	$^{+0.0017}_{-0.0014}$	$^{+0.0016}_{-0.0014}$	$^{+0.0021}_{-0.0018}$	$^{+0.0027}_{-0.0022}$	$^{+0.0015}_{-0.0013}$	$^{+0.0022}_{-0.0019}$	$^{+0.0027}_{-0.0023}$	$^{+0.0027}_{-0.0023}$	$^{+0.0037}_{-0.0031}$
Experimental	$^{+0.0033}_{-0.0034}$	$^{+0.0037}_{-0.0037}$	$^{+0.0036}_{-0.0037}$	$^{+0.0037}_{-0.0038}$	$^{+0.0038}_{-0.0038}$	$^{+0.0033}_{-0.0034}$	$^{+0.0036}_{-0.0037}$	$^{+0.0036}_{-0.0036}$	$^{+0.0036}_{-0.0037}$	$^{+0.0037}_{-0.0038}$	$^{+0.0033}_{-0.0034}$	$^{+0.0037}_{-0.0037}$	$^{+0.0037}_{-0.0037}$	$^{+0.0037}_{-0.0037}$	$^{+0.0038}_{-0.0038}$
Total theory	$^{+0.0017}_{-0.0017}$	$^{+0.0028}_{-0.0029}$	$^{+0.0040}_{-0.0042}$	$^{+0.0065}_{-0.0065}$	$^{+0.0078}_{-0.0074}$	$^{+0.0024}_{-0.0024}$	$^{+0.0027}_{-0.0028}$	$^{+0.0032}_{-0.0032}$	$^{+0.0042}_{-0.0041}$	$^{+0.0053}_{-0.0051}$	$^{+0.0017}_{-0.0015}$	$^{+0.0028}_{-0.0026}$	$^{+0.0039}_{-0.0036}$	$^{+0.0050}_{-0.0047}$	$^{+0.0070}_{-0.0064}$
$s_0 \in [2.50, M_\tau^2]$	0.0032	0.0070	0.0117	0.0188	0.0229	0.0042	0.0089	0.0122	0.0146	0.0200	0.0034	0.0074	0.0126	0.0204	0.0272
Total	$^{+0.0049}_{-0.0050}$	$^{+0.0084}_{-0.0085}$	$^{+0.0129}_{-0.0129}$	$^{+0.0203}_{-0.0203}$	$^{+0.0245}_{-0.0244}$	$^{+0.0058}_{-0.0059}$	$^{+0.0100}_{-0.0100}$	$^{+0.0131}_{-0.0131}$	$^{+0.0156}_{-0.0156}$	$^{+0.0210}_{-0.0210}$	$^{+0.0051}_{-0.0050}$	$^{+0.0088}_{-0.0087}$	$^{+0.0137}_{-0.0136}$	$^{+0.0213}_{-0.0213}$	$^{+0.0283}_{-0.0282}$

TABLE XXI. Determination of $|V_{us}|$ in different schemes from the OPAL data using prescription II. The longitudinal component is calculated using the pQCD Adler function.

	$\lvert V_{us}\rvert_{\mathrm{CIPT}}$					$\lvert V_{us}\rvert_{\mathrm{FOPT}}$					$\lvert V_{us}\rvert_{\mathrm{RGSPT}}$				
Parameters	(0, 0)	(1, 0)	(2, 0)	(3, 0)	(4, 0)	(0, 0)	(1, 0)	(2, 0)	(3, 0)	(4, 0)	(0, 0)	(1, 0)	(2, 0)	(3, 0)	(4, 0)
$\lvert V_{us}\rvert$ (central)	0.2217	0.2239	0.2275	0.2341	0.2452	0.2227	0.2246	0.2271	0.2310	0.2365	0.2221	0.2246	0.2286	0.2358	0.2477
m_s	$^{+0.0014}_{-0.0012}$	$^{+0.0025}_{-0.0021}$	$^{+0.0043}_{-0.0036}$	$^{+0.0072}_{-0.0059}$	$^{+0.0126}_{-0.0097}$	$^{+0.0017}_{-0.0015}$	$^{+0.0028}_{-0.0024}$	$^{+0.0042}_{-0.0035}$	$^{+0.0062}_{-0.0051}$	$^{+0.0090}_{-0.0072}$	$^{+0.0015}_{-0.0013}$	$^{+0.0027}_{-0.0023}$	$^{+0.0047}_{-0.0039}$	$^{+0.0079}_{-0.0064}$	$^{+0.0138}_{-0.0105}$
Experimental	$^{+0.0033}_{-0.0034}$	$^{+0.0037}_{-0.0038}$	$^{+0.0037}_{-0.0038}$	$^{+0.0039}_{-0.0040}$	$^{+0.0042}_{-0.0043}$	$^{+0.0033}_{-0.0034}$	$^{+0.0037}_{-0.0038}$	$^{+0.0037}_{-0.0038}$	$^{+0.0039}_{-0.0039}$	$^{+0.0041}_{-0.0041}$	$^{+0.0033}_{-0.0034}$	$^{+0.0037}_{-0.0038}$	$^{+0.0038}_{-0.0038}$	$^{+0.0039}_{-0.0040}$	$^{+0.0043}_{-0.0043}$
Total theory	$^{+0.0017}_{-0.0017}$	$^{+0.0033}_{-0.0035}$	$^{+0.0063}_{-0.0065}$	$^{+0.0121}_{-0.0116}$	$^{+0.0237}_{-0.0206}$	$^{+0.0024}_{-0.0024}$	$^{+0.0043}_{-0.0043}$	$^{+0.0071}_{-0.0068}$	$^{+0.0110}_{-0.0102}$	$^{+0.0165}_{-0.0147}$	$^{+0.0017}_{-0.0015}$	$^{+0.0033}_{-0.0030}$	$^{+0.0061}_{-0.0055}$	$^{+0.0109}_{-0.0096}$	$^{+0.0200}_{-0.0168}$
$s_0 \in [2.50, M_\tau^2]$	0.0030	0.0070	0.0117	0.0188	0.0313	0.0042	0.0089	0.0143	0.0216	0.0325	0.0032	0.0074	0.0126	0.0204	0.0338
Total	$^{+0.0048}_{-0.0048}$	$^{+0.0086}_{-0.0087}$	$^{+0.0138}_{-0.0139}$	$^{+0.0227}_{-0.0225}$	$^{+0.0395}_{-0.0377}$	$^{+0.0058}_{-0.0059}$	$^{+0.0106}_{-0.0162}$	$^{+0.0164}_{-0.0163}$	$^{+0.0245}_{-0.0242}$	$^{+0.0368}_{-0.0359}$	$^{+0.0049}_{-0.0049}$	$^{+0.0089}_{-0.0089}$	$^{+0.0145}_{-0.0145}$	$^{+0.0235}_{-0.0229}$	$^{+0.0395}_{-0.0380}$

TABLE XXII. Determination of $|V_{us}|$ in different schemes from the OPAL data using prescription I. The phenomenological contributions are used for longitudinal components.

	$\|V_{us}\|_{\mathrm{CIPT}}$					$\|V_{us}\|_{\mathrm{FOPT}}$					$\|V_{us}\|_{\mathrm{RGSPT}}$				
Parameters	(0, 0)	(1, 0)	(2, 0)	(3, 0)	(4, 0)	(0, 0)	(1, 0)	(2, 0)	(3, 0)	(4, 0)	(0, 0)	(1, 0)	(2, 0)	(3, 0)	(4, 0)
$\|V_{us}\|$ (central)	0.2211	0.2210	0.2212	0.2228	0.2226	0.2222	0.2224	0.2225	0.2208	0.2177	0.2213	0.2213	0.2219	0.2238	0.2233
m_s	$^{+0.0005}_{-0.0004}$	$^{+0.0010}_{-0.0009}$	$^{+0.0018}_{-0.0015}$	$^{+0.0029}_{-0.0025}$	$^{+0.0036}_{-0.0030}$	$^{+0.0008}_{-0.0007}$	$^{+0.0014}_{-0.0012}$	$^{+0.0022}_{-0.0019}$	$^{+0.0024}_{-0.0021}$	$^{+0.0022}_{-0.0019}$	$^{+0.0005}_{-0.0004}$	$^{+0.0011}_{-0.0009}$	$^{+0.0019}_{-0.0017}$	$^{+0.0032}_{-0.0028}$	$^{+0.0038}_{-0.0032}$
Experimental	$^{+0.0033}_{-0.0034}$	$^{+0.0036}_{-0.0037}$	$^{+0.0036}_{-0.0037}$	$^{+0.0037}_{-0.0038}$	$^{+0.0038}_{-0.0038}$	$^{+0.0033}_{-0.0034}$	$^{+0.0037}_{-0.0037}$	$^{+0.0037}_{-0.0037}$	$^{+0.0037}_{-0.0037}$	$^{+0.0037}_{-0.0038}$	$^{+0.0033}_{-0.0034}$	$^{+0.0036}_{-0.0037}$	$^{+0.0036}_{-0.0037}$	$^{+0.0037}_{-0.0038}$	$^{+0.0038}_{-0.0039}$
Total theory	$^{+0.0005}_{-0.0005}$	$^{+0.0010}_{-0.0010}$	$^{+0.0020}_{-0.0020}$	$^{+0.0036}_{-0.0037}$	$^{+0.0053}_{-0.0054}$	$^{+0.0009}_{-0.0009}$	$^{+0.0019}_{-0.0019}$	$^{+0.0033}_{-0.0033}$	$^{+0.0039}_{-0.0039}$	$^{+0.0043}_{-0.0041}$	$^{+0.0005}_{-0.0004}$	$^{+0.0011}_{-0.0010}$	$^{+0.0022}_{-0.0020}$	$^{+0.0040}_{-0.0036}$	$^{+0.0055}_{-0.0050}$
$s_0 \in [2.5, M_\tau^2]$	0.0032	0.0070	0.0117	0.0188	0.0229	0.0042	0.0089	0.0122	0.0146	0.0200	0.0034	0.0074	0.0126	0.0204	0.0272
Total	$^{+0.0047}_{-0.0047}$	$^{+0.0080}_{-0.0080}$	$^{+0.0124}_{-0.0124}$	$^{+0.0195}_{-0.0195}$	$^{+0.0238}_{-0.0239}$	$^{+0.0054}_{-0.0054}$	$^{+0.0098}_{-0.0099}$	$^{+0.0131}_{-0.0132}$	$^{+0.0155}_{-0.0155}$	$^{+0.0208}_{-0.0207}$	$^{+0.0048}_{-0.0048}$	$^{+0.0084}_{-0.0084}$	$^{+0.0133}_{-0.0133}$	$^{+0.0211}_{-0.0211}$	$^{+0.0280}_{-0.0279}$

TABLE XXIII. Determination of $|V_{us}|$ from OPAL data using prescription II. The phenomenological contributions are used for longitudinal components.

	$\|V_{us}\|_{\mathrm{CIPT}}$					$\|V_{us}\|_{\mathrm{FOPT}}$					$\|V_{us}\|_{\mathrm{RGSPT}}$				
Parameters	(0, 0)	(1, 0)	(2, 0)	(3, 0)	(4, 0)	(0, 0)	(1, 0)	(2, 0)	(3, 0)	(4, 0)	(0, 0)	(1, 0)	(2, 0)	(3, 0)	(4, 0)
$\|V_{us}\|$ (central)	0.2211	0.2210	0.2212	0.2228	0.2260	0.2222	0.2224	0.2225	0.2236	0.2253	0.2213	0.2213	0.2219	0.2238	0.2274
m_s	$^{+0.0005}_{-0.0004}$	$^{+0.0010}_{-0.0009}$	$^{+0.0018}_{-0.0015}$	$^{+0.0029}_{-0.0025}$	$^{+0.0039}_{-0.0046}$	$^{+0.0008}_{-0.0007}$	$^{+0.0014}_{-0.0012}$	$^{+0.0022}_{-0.0019}$	$^{+0.0032}_{-0.0027}$	$^{+0.0045}_{-0.0038}$	$^{+0.0005}_{-0.0004}$	$^{+0.0011}_{-0.0009}$	$^{+0.0019}_{-0.0017}$	$^{+0.0032}_{-0.0028}$	$^{+0.0051}_{-0.0043}$
Experimental	$^{+0.0033}_{-0.0034}$	$^{+0.0036}_{-0.0037}$	$^{+0.0036}_{-0.0037}$	$^{+0.0037}_{-0.0038}$	$^{+0.0038}_{-0.0039}$	$^{+0.0033}_{-0.0034}$	$^{+0.0037}_{-0.0037}$	$^{+0.0037}_{-0.0037}$	$^{+0.0037}_{-0.0038}$	$^{+0.0038}_{-0.0039}$	$^{+0.0033}_{-0.0034}$	$^{+0.0036}_{-0.0037}$	$^{+0.0036}_{-0.0037}$	$^{+0.0037}_{-0.0038}$	$^{+0.0039}_{-0.0039}$
Total theory	$^{+0.0005}_{-0.0005}$	$^{+0.0010}_{-0.0010}$	$^{+0.0020}_{-0.0020}$	$^{+0.0036}_{-0.0037}$	$^{+0.0062}_{-0.0065}$	$^{+0.0009}_{-0.0009}$	$^{+0.0019}_{-0.0019}$	$^{+0.0033}_{-0.0033}$	$^{+0.0051}_{-0.0050}$	$^{+0.0074}_{-0.0071}$	$^{+0.0005}_{-0.0004}$	$^{+0.0011}_{-0.0010}$	$^{+0.0022}_{-0.0020}$	$^{+0.0040}_{-0.0036}$	$^{+0.0068}_{-0.0061}$
$s_0 \in [2.5, M_\tau^2]$	0.0030	0.0070	0.0117	0.0188	0.0313	0.0042	0.0089	0.0143	0.0216	0.0325	0.0032	0.0074	0.0126	0.0204	0.0338
Total	$^{+0.0045}_{-0.0045}$	$^{+0.0080}_{-0.0080}$	$^{+0.0124}_{-0.0124}$	$^{+0.0195}_{-0.0196}$	$^{+0.0321}_{-0.0322}$	$^{+0.0054}_{-0.0054}$	$^{+0.0098}_{-0.0099}$	$^{+0.0151}_{-0.0151}$	$^{+0.0225}_{-0.0225}$	$^{+0.0336}_{-0.0335}$	$^{+0.0046}_{-0.0047}$	$^{+0.0084}_{-0.0084}$	$^{+0.0133}_{-0.0133}$	$^{+0.0211}_{-0.0211}$	$^{+0.0347}_{-0.0346}$

[1] M. Davier, A. Hocker, and Z. Zhang, Rev. Mod. Phys. **78**, 1043 (2006).
[2] A. Pich, Prog. Part. Nucl. Phys. **75**, 41 (2014).
[3] K. G. Wilson, Phys. Rev. **179**, 1499 (1969).
[4] J. Gasser and H. Leutwyler, Nucl. Phys. **B250**, 465 (1985).
[5] S. Aoki *et al.* (Flavour Lattice Averaging Group), Eur. Phys. J. C **80**, 113 (2020).
[6] J. L. Kneur and A. Neveu, Phys. Rev. D **101**, 074009 (2020).
[7] J. L. Kneur and A. Neveu, Phys. Rev. D **92**, 074027 (2015).
[8] D. Boito, I. Caprini, M. Golterman, K. Maltman, and S. Peris, Phys. Rev. D **97**, 054007 (2018).
[9] K. G. Chetyrkin, Phys. Lett. B **390**, 309 (1997).
[10] C. Becchi, S. Narison, E. de Rafael, and F. J. Yndurain, Z. Phys. C **8**, 335 (1981).
[11] D. J. Broadhurst, Phys. Lett. **101B**, 423 (1981).
[12] S. G. Gorishnii, A. L. Kataev, S. A. Larin, and L. R. Surguladze, Mod. Phys. Lett. A **05**, 2703 (1990).
[13] S. G. Gorishnii, A. L. Kataev, S. A. Larin, and L. R. Surguladze, Phys. Rev. D **43**, 1633 (1991).
[14] P. A. Baikov, K. G. Chetyrkin, and J. H. Kuhn, Phys. Rev. Lett. **96**, 012003 (2006).
[15] E. Gamiz, M. Jamin, A. Pich, J. Prades, and F. Schwab, J. High Energy Phys. 01 (**2003**) 060.
[16] K. Maltman and J. Kambor, Phys. Rev. D **64**, 093014 (2001).
[17] K. Maltman and J. Kambor, Phys. Rev. D **65**, 074013 (2002).
[18] M. Jamin, J. A. Oller, and A. Pich, Nucl. Phys. **B622**, 279 (2002).
[19] M. Jamin, J. A. Oller, and A. Pich, Eur. Phys. J. C **24**, 237 (2002).
[20] B. Ananthanarayan and D. Das, Phys. Rev. D **94**, 116014 (2016).
[21] E. Braaten, S. Narison, and A. Pich, Nucl. Phys. **B373**, 581 (1992).
[22] A. Pich and J. Prades, J. High Energy Phys. 10 (1999) 004.
[23] S. Narison and A. Pich, Phys. Lett. B **211**, 183 (1988).
[24] F. Le Diberder and A. Pich, Phys. Lett. B **289**, 165 (1992).
[25] K. Ackerstaff *et al.* (OPAL Collaboration), Eur. Phys. J. C **7**, 571 (1999); The nonstrange spectral function is available at https://www.mpp.mpg.de/~menke/?q=OPAL.
[26] M. Davier, A. Höcker, B. Malaescu, C. Z. Yuan, and Z. Zhang, Eur. Phys. J. C **74**, 2803 (2014).
[27] G. Abbiendi *et al.* (OPAL Collaboration), Eur. Phys. J. C **35**, 437 (2004).
[28] D. Boito, M. Golterman, K. Maltman, S. Peris, M. V. Rodrigues, and W. Schaaf, Phys. Rev. D **103**, 034028 (2021).
[29] E. Braaten and C. S. Li, Phys. Rev. D **42**, 3888 (1990).

[30] J. Erler, Rev. Mex. Fis. **50**, 200 (2004).
[31] R. Barate *et al.* (ALEPH Collaboration), Eur. Phys. J. C **11**, 599 (1999).
[32] S. Chen, M. Davier, E. Gamiz, A. Hocker, A. Pich, and J. Prades, Eur. Phys. J. C **22**, 31 (2001).
[33] P. A. Zyla *et al.* (Particle Data Group), Prog. Theor. Exp. Phys. **2020**, 083C01 (2020).
[34] A. H. Hoang, C. Lepenik, and V. Mateu, Comput. Phys. Commun. **270**, 108145 (2022).
[35] M. R. Ahmady, F. A. Chishtie, V. Elias, and T. G. Steele, Phys. Lett. B **479**, 201 (2000).
[36] M. R. Ahmady, F. A. Chishtie, V. Elias, A. H. Fariborz, N. Fattahi, D. G. C. McKeon, T. N. Sherry, and T. G. Steele, Phys. Rev. D **66**, 014010 (2002).
[37] M. R. Ahmady, F. A. Chishtie, V. Elias, A. H. Fariborz, D. G. C. McKeon, T. N. Sherry, A. Squires, and T. G. Steele, Phys. Rev. D **67**, 034017 (2003).
[38] G. Abbas, B. Ananthanarayan, and I. Caprini, Phys. Rev. D **85**, 094018 (2012).
[39] B. Ananthanarayan, D. Das, and M. S. A. Alam Khan, Phys. Rev. D **102**, 076008 (2020).
[40] G. Abbas, A. Jain, V. Singh, and N. Singh, arXiv: 2205.06061.
[41] T. Appelquist and H. Georgi, Phys. Rev. D **8**, 4000 (1973).
[42] A. Zee, Phys. Rev. D **8**, 4038 (1973).
[43] K. G. Chetyrkin, A. L. Kataev, and F. V. Tkachov, Phys. Lett. B **85**, 277 (1979).
[44] M. Dine and J. R. Sapirstein, Phys. Rev. Lett. **43**, 668 (1979).
[45] S. G. Gorishnii, A. L. Kataev, and S. A. Larin, Phys. Lett. B **259**, 144 (1991).
[46] L. R. Surguladze and M. A. Samuel, Phys. Rev. Lett. **66**, 560 (1991); **66**, 2416(E) (1991).
[47] K. G. Chetyrkin, Phys. Lett. B **391**, 402 (1997).
[48] P. A. Baikov, K. G. Chetyrkin, and J. H. Kuhn, Phys. Rev. Lett. **101**, 012002 (2008).
[49] P. A. Baikov, K. G. Chetyrkin, and J. H. Kuhn, Phys. Rev. Lett. **104**, 132004 (2010).
[50] F. Herzog, B. Ruijl, T. Ueda, J. A. M. Vermaseren, and A. Vogt, J. High Energy Phys. 08 (2017) 113.
[51] P. A. Baikov, K. G. Chetyrkin, and J. H. Kuhn, Phys. Rev. Lett. **95**, 012003 (2005).
[52] S. C. Generalis, J. Phys. G **15**, L225 (1989).
[53] K. G. Chetyrkin and A. Kwiatkowski, Z. Phys. C **59**, 525 (1993).
[54] P. A. Baikov, K. G. Chetyrkin, and J. H. Kuhn, Nucl. Phys. B, Proc. Suppl. **135**, 243 (2004).
[55] S. G. Gorishnii, A. L. Kataev, and S. A. Larin, Nuovo Cimento A **92**, 119 (1986).
[56] W. Bernreuther and W. Wetzel, Z. Phys. C **11**, 113 (1981).
[57] A. Pich and J. Prades, J. High Energy Phys. 06 (1998) 013.
[58] K. G. Chetyrkin, V. P. Spiridonov, and S. G. Gorishnii, Phys. Lett. **160B**, 149 (1985).
[59] R. M. Albuquerque, S. Narison, and M. Nielsen, Phys. Lett. B **684**, 236 (2010).
[60] H. Leutwyler, NATO Sci. Ser. B **363**, 149 (1997).
[61] A. Pich, Prog. Part. Nucl. Phys. **117**, 103846 (2021).
[62] M. Beneke and M. Jamin, J. High Energy Phys. 09 (2008) 044.
[63] S. Schael *et al.* (ALEPH Collaboration), Phys. Rep. **421**, 191 (2005).
[64] M. Davier, S. Descotes-Genon, A. Hocker, B. Malaescu, and Z. Zhang, Eur. Phys. J. C **56**, 305 (2008).
[65] Y. S. Amhis *et al.* (HFLAV Collaboration), Eur. Phys. J. C **81**, 226 (2021).
[66] K. Maltman and C. E. Wolfe, Phys. Lett. B **650**, 27 (2007).
[67] E. Gamiz, M. Jamin, A. Pich, J. Prades, and F. Schwab, Phys. Rev. Lett. **94**, 011803 (2005).
[68] E. Gamiz, M. Jamin, A. Pich, J. Prades, and F. Schwab, Nucl. Phys. B, Proc. Suppl. **169**, 85 (2007).
[69] E. Gamiz, M. Jamin, A. Pich, J. Prades, and F. Schwab, Nucl. Phys. B, Proc. Suppl. **144**, 59 (2005).
[70] E. Gamiz, M. Jamin, A. Pich, J. Prades, and F. Schwab, arXiv:hep-ph/0505122.
[71] L. E. Adam and K. G. Chetyrkin, Phys. Lett. B **329**, 129 (1994).
[72] L. V. Lanin, V. P. Spiridonov, and K. G. Chetyrkin, Yad. Fiz. **44**, 1372 (1986).
[73] D. Boito, D. Hornung, and M. Jamin, J. High Energy Phys. 12 (2015) 090.
[74] M. A. Shifman, A. I. Vainshtein, and V. I. Zakharov, Nucl. Phys. **B147**, 519 (1979).
[75] J. Kambor and K. Maltman, Phys. Rev. D **62**, 093023 (2000).
[76] K. Maltman and C. E. Wolfe, Phys. Lett. B **639**, 283 (2006).
[77] R. J. Hudspith, R. Lewis, K. Maltman, and J. Zanotti, Phys. Lett. B **781**, 206 (2018).
[78] D. J. Gross and F. Wilczek, Phys. Rev. Lett. **30**, 1343 (1973).
[79] W. E. Caswell, Phys. Rev. Lett. **33**, 244 (1974).
[80] D. R. T. Jones, Nucl. Phys. **B75**, 531 (1974).
[81] O. V. Tarasov, A. A. Vladimirov, and A. Y. Zharkov, Phys. Lett. **93B**, 429 (1980).
[82] S. A. Larin and J. A. M. Vermaseren, Phys. Lett. B **303**, 334 (1993).
[83] T. van Ritbergen, J. A. M. Vermaseren, and S. A. Larin, Phys. Lett. B **400**, 379 (1997).
[84] M. Czakon, Nucl. Phys. **B710**, 485 (2005).
[85] P. A. Baikov, K. G. Chetyrkin, and J. H. Kühn, Phys. Rev. Lett. **118**, 082002 (2017).
[86] F. Herzog, B. Ruijl, T. Ueda, J. Vermaseren, and A. Vogt, J. High Energy Phys. 02 (**2017**) 090.
[87] T. Luthe, A. Maier, P. Marquard, and Y. Schröder, J. High Energy Phys. 01 (2017) 081.
[88] R. Tarrach, Nucl. Phys. **B183**, 384 (1981).
[89] O. V. Tarasov, Phys. Part. Nucl. Lett. **17**, 109 (2020).
[90] S. A. Larin, Phys. Lett. B **303**, 113 (1993).
[91] J. A. M. Vermaseren, S. A. Larin, and T. van Ritbergen, Phys. Lett. B **405**, 327 (1997).
[92] K. G. Chetyrkin, Phys. Lett. B **404**, 161 (1997).
[93] P. A. Baikov, K. G. Chetyrkin, and J. H. Kühn, J. High Energy Phys. 10 (2014) 076.
[94] T. Luthe, A. Maier, P. Marquard, and Y. Schröder, J. High Energy Phys. 07 (2016) 127.
[95] P. A. Baikov and K. G. Chetyrkin, Proc. Sci., RADCOR2017 (**2018**) 025.
[96] P. Pascual and E. de Rafael, Z. Phys. C **12**, 127 (1982).
[97] M. Jamin and M. Munz, Z. Phys. C **60**, 569 (1993).

[98] S. C. Generalis, J. Phys. G **16**, 785 (1990).
[99] L. R. Surguladze and F. V. Tkachov, Nucl. Phys. **B331**, 35 (1990).
[100] E. Bagan, J. I. Latorre, and P. Pascual, Z. Phys. C **32**, 43 (1986).
[101] D. J. Broadhurst and S. C. Generalis, Phys. Lett. **165B**, 175 (1985).
[102] S. C. Generalis, J. Phys. G **16**, 367 (1990).
[103] G. T. Loladze, L. R. Surguladze, and F. V. Tkachov, Phys. Lett. **162B**, 363 (1985).